NMR Structural Studies of a 15-mer DNA Sequence from a *ras* Protooncogene, Modified at the First Base of Codon 61 with the Carcinogen 4-Aminobiphenyl

Bongsup P. Cho,*,‡,§ Frederick A. Beland,*,‡ and M. Matilde Marques*,‖

Division of Biochemical Toxicology, National Center for Toxicological Research, Jefferson, Arkansas 72079, and Centro de Quimica Estrutural, Complexo I, IST, Av. Rovisco Pais, 1096 Lisboa Codex, Portugal

Received May 20, 1992; Revised Manuscript Received July 30, 1992

ABSTRACT: Proton NMR studies were conducted on the complementary 15-mer duplex d(5′-TACTCT-TCTTGACCT)·(5′-AGGTCAAGAAGAGTA) (designated as unmodified 15-mer duplex) spanning a portion of the mouse c-Ha-*ras* protooncogene centered around codon 61. Identical studies were carried out on the same sequence, after specific modification with a reactive derivative of the carcinogen 4-aminobiphenyl (ABP), which resulted in incorporation of a single *N*-(deoxyguanosin-8-yl)-4-aminobiphenyl (dG-C8-ABP) adduct in the noncoding strand (designated as ABP-modified 15-mer duplex). The adduct was located at the position corresponding to the first base of codon 61. The NMR data for the unmodified 15-mer duplex were fully consistent with a standard right-handed B-type DNA duplex conformation, with the possible exception of the frayed terminal base pairs. The ABP-modified 15-mer duplex was found to adopt one major conformation, although at least one additional conformation could be detected especially near room temperature. The major form, which exhibited strikingly similar NOE patterns as to those of the parent oligomer, both in H_2O and D_2O spectra, assumed a standard Watson–Crick base pairing throughout the entire length of the duplex, including the modification site and its flanking base pairs. Although some local perturbation of the helix could be detected in the vicinity of the modified guanosine, the NOE distance constraints established that the helix was globally right-handed and that the glycosidic torsion angles had the normal anti orientation, both at the modified base and its partner cytidine. Furthermore, the absence of strong NOE interactions between protons in the ABP moiety, which was rapidly rotating, and the nucleic acid protons was consistent with positioning of the arylamine moiety in the major groove of a weakly distorted double-helical structure. Although insufficient data prevented a detailed characterization of the minor conformer(s), the observation of significant shieldings for all the arylamine protons indicated a different orientation at the modified site in the minor contributor(s), possibly with extensive stacking between the ABP fragment and the neighboring bases.

A large number of arylamines and their derivatives are well established carcinogens, as a result of metabolic activation to reactive electrophiles that are capable of forming covalent adducts with DNA. According to most studies, the major and most persistent adducts found after in vivo administration of arylamine and arylamide carcinogens are C8-substituted deoxyguanosine derivatives (Beland & Kadlubar, 1990). The formation of these chemical lesions is thought to be a critical step in the carcinogenic process, possibly leading to mutagenic activation of oncogenes (Anderson & Reynolds, 1989). Therefore, elucidation of the conformational alterations that arise from chemical modification of DNA should be important for understanding subsequent events, such as replication, repair, and mutation induction.

This problem has been addressed most extensively using 2-aminofluorene (AF)[1] derivatives by a variety of experimental techniques. Spectroscopic methods (Sage & Leng, 1980; Santella et al., 1981; Sanford & Krugh, 1985), including high-resolution NMR (Leng et al., 1980; Evans et al., 1980, 1984; Evans & Miller, 1982; Neidle et al., 1984; Evans & Levine, 1986, 1988; Krugh et al., 1987) and potential energy calculations (Lipkowitz et al., 1982; Hingerty & Broyde, 1982, 1986; Broyde & Hingerty, 1987), have consistently suggested that *N*-(deoxyguanosin-8-yl)-2-acetylaminofluorene (dG-C8-AAF), the main adduct resulting from in vitro modification of DNA by reactive 2-acetylaminofluorene (AAF) derivatives, preferentially adopts a syn conformation about the glycosyl bond. This departure from the normal anti conformation has significant structural consequences, resulting in displacement of the modified guanosine from the standard right-handed helix and stacking of the AAF chromophore with the neighboring bases. The unacetylated adduct *N*-(deoxyguanosin-8-yl)-2-aminofluorene (dG-C8-AF), which is more persistent in vivo than its acetylated counterpart (Beland & Kadlubar, 1990), has been shown to cause less helix perturbation (Sage & Leng, 1980; Leng et al., 1980; van Houte et al., 1987, 1988). Theoretical studies (Lipkowitz et al., 1982; Broyde & Hingerty, 1983; Hingerty & Broyde, 1986) have supported the existence of several low-energy conformers in which the modified guanosines remain in an anti conformation and the AF-chromophore resides in the major groove of a weakly distorted duplex. However, evidence for an AF-modified syn guanosine, with the AF fragment in the minor groove of a right-handed helix, has recently been presented

* Correspondence can be addressed to any of the authors.
‡ National Center for Toxicological Research.
§ Current address: Department of Medicinal Chemistry, College of Pharmacy, University of Rhode Island, Kingston, RI 02881.
‖ Centro de Quimica Estrutural.

[1] Abbreviations: AAF, 2-acetylaminofluorene; ABP, 4-aminobiphenyl; AF, 2-aminofluorene; A_{260}, absorbance at 260 nm; COSY, correlation spectroscopy; dG-C8-AAF, *N*-(deoxyguanosin-8-yl)-2-acetylaminofluorene; dG-C8-ABP, *N*-(deoxyguanosin-8-yl)-4-aminobiphenyl; dG-C8-AF, *N*-(deoxyguanosin-8-yl)-2-aminofluorene; EDTA, ethylenediaminetetraacetic acid; FID, free induction decay; NMR, nuclear magnetic resonance; NOE, nuclear Overhauser effect; 1D, one dimensional; TMS, tetramethylsilane; TPPI, time-proportional phase increment; TSP, 3-(trimethylsilyl)propionate-*2,2,3,3-d*$_4$; 2D, two dimensional; NOESY, nuclear Overhauser effect spectroscopy.

0006-2960/92/0431-9587$03.00/0

in a combined high-resolution NMR and computational study of a 12-mer DNA duplex containing a G:A base pair at the modification site (Norman et al., 1989).

4-Aminobiphenyl (ABP) is a bladder carcinogen to which human populations are widely exposed from a variety of sources, including cigarette smoke (Patrianakos & Hoffmann, 1979; Vineis, 1992). ABP is structurally similar to AF, from which it differs by the lack of one methylene bridge and, consequently, the absence of planarity in the aromatic ring. Despite the structural similarity, the mutagenicities and the organ specificities in experimental animals of these two carcinogens are considerably different (Beland & Kadlubar, 1990). Therefore, the nature of the arylamine moieties appears to play a significant role in their biological effects. Studies on the conformational properties of the major ABP-derived DNA adduct, *N*-(deoxyguanosin-8-yl)-4-aminobiphenyl (dG-C8-ABP), are limited (Kadlubar et al., 1982; Shapiro et al., 1986; Abuaf et al., 1987; Lasko et al., 1987). NMR coupling constants associated with the sugar ring of dG-C8-ABP (Kadlubar et al., 1982) are consistent with those observed for dG-C8-AF (Evans et al., 1980), which suggests a similar sugar ring conformation and a comparable accessibility of the anti conformation about the glycosyl bond. In agreement with this, NMR and theoretical work on the ABP-modified single-strand dimer d(Cp[ABP]G) have suggested that the dG-C8-ABP adduct may be accommodated in the major groove of a weakly distorted duplex DNA (Broyde et al., 1985; Shapiro et al., 1986). This has subsequently been supported by the studies on a single-strand tetramer containing one dG-C8-ABP residue, which could be efficiently incorporated into a viral genome (Lasko et al., 1987). Theoretical studies have also shown that similar low-energy conformers exist for AF- and ABP-modified guanosines, although subtle differences in the stacking ability of the two arylamine fragments were detected, with the ABP adduct overlapping less efficiently with the nearby bases (Shapiro et al., 1986). This difference in stacking was suggested to account for the lower frame-shift mutagenicity of dG-C8-ABP compared to dG-C8-AF in *Salmonella typhimurium* TA1538. It was also proposed to be responsible for the relative resistance of dG-C8-ABP to DNA repair enzymes in the liver of dogs (Beland & Kadlubar, 1990).

NMR structural studies on DNA duplexes modified by arylamines have been limited because of spectral complexity. Earlier work on an AAF-modified 9-mer (Krugh et al., 1987), which globally retained a right-handed form, indicated the adoption of a syn conformation by the modified guanosine, but further structural details about the vicinity of the adduct site were not established. The previously cited study by Norman et al. (1989) on a 12-mer DNA duplex containing an AF-modified syn guanosine opposing an anti adenosine represented the first thorough characterization of one of these systems. Similar NMR studies of duplexes with a natural [AF]G:C base pair at the modification site have not been described.

We have recently reported (Marques & Beland, 1990) the synthesis and chemical characterization of a complementary 15-mer DNA duplex, d(5'-TACTCTTCTTGACCT)·d(5'-AGGTCAAGAAGAGTA), spanning a portion of the mouse c-Ha-*ras* protooncogene centered around codon 61 and selectively modified to give dG-C8-AF or dG-C8-ABP at the guanosine corresponding to the first base of codon 61. dG-C8-AF and dG-C8-ABP are the major DNA adducts detected in mouse liver during the administration of hepatocarcinogenic regimens of AAF and ABP, respectively (Poirier et al., 1991; Beland et al., 1992). Furthermore, the guanosine located at the first base of codon 61 is the site of a G → T transversion associated with the induction of hepatomas in male B6C3F1 mice treated with AAF derivatives (Wiseman et al., 1986). Although similar experiments do not appear to have been conducted with ABP, a comparison of adduct concentrations obtained during tumorigenic dosing regimens suggests that dG-C8-AF is more efficient than dG-C8-ABP at inducing hepatic tumors in mice, which may be due to conformational differences between the adducts (Beland et al., 1992). Our preliminary results, based on thermal denaturation experiments and circular dichroism studies, indicated that the two modified 15-mer sequences form stable duplexes with an overall right-handed B-type conformation (Marques & Beland, 1990). In this paper, we report a comparative two-dimensional (2D) NMR study of the parent 15-mer duplex and its ABP-modified analogue, in order to gain detailed insight on the local structural effects of dG-C8-ABP.

MATERIALS AND METHODS

Chemicals. ABP was purchased from Aldrich Chemical Co., Milwaukee, WI. dG-C8-ABP was prepared as described in Famulok et al. (1989). The synthesis and chemical characterization of the coding and noncoding 15-mer strands and selective ABP-modification of the noncoding strand have been reported (Marques & Beland, 1990).

Sample Preparation. Prior to duplex formation, each 15-mer was dissolved in 100 mM NaCl, 10 mM sodium phosphate, and 100 μM disodium EDTA, pH 7.0, loaded on Waters Sep-Pak C18 reversed-phase cartridges [50 absorption units (A_{260})/cartridge], washed with water, and recovered in its sodium form with 40% acetonitrile in water.

Duplexes for NMR experiments were subsequently obtained in 1:1 molar strand ratios on the basis of our previously reported extinction coefficients at 260 nm (Marques & Beland, 1990). The unmodified duplex was thus prepared by mixing 194A_{260} of the coding strand, d(AGGTCAAGAAGAGTA), and 149A_{260} of the corresponding noncoding strand, d(TACTCT-TCTTGACCT), in 500 μL of NMR buffer, consisting of 100 mM NaCl, 10 mM sodium phosphate, and 100 μM disodium EDTA, pH 7.0. The ABP-modified duplex was similarly prepared by mixing 120A_{260} of the coding strand and 103A_{260} of the ABP-modified strand, d(TACTCTTCTT[ABP]GAC-CT). Each solution was maintained at 60 °C for 1 h and then kept at 5 °C for 24 h, to ensure complete annealing. The buffered NMR samples required for analysis of the nonexchangeable protons were lyophilized three times from 99.96% D_2O and finally adjusted to 350 μL with 99.996% D_2O (designated as D_2O buffer). For observation of the exchangeable protons, the samples were dissolved in the same volume of 90% H_2O/10% D_2O (v/v) (designated as H_2O buffer). The solutions were degassed with argon before capping.

NMR Experiments. All NMR spectra were obtained in the proton configuration on a Bruker AM500 spectrometer operating at 500 MHz. Spectra were recorded in the temperature range of 5–67 °C, as is further described in the text. Probe temperatures were calibrated using deuterated methanol (Van Geet, 1968). Chemical shifts are reported in ppm downfield from 3-(trimethylsilyl)propionate-*2,2,3,3-d*$_4$ (TSP).

For observation of the exchangeable protons, one-dimensional (1D) proton spectra in H_2O buffer were collected with 16K data points over a 11 111-Hz sweep width. The H_2O peak was suppressed by using a 1331 pulse sequence (Hore,

1983) with the carrier frequency set on the H_2O resonance. 1D NOE difference experiments in H_2O buffer were carried out using the same NMR parameters, with resonances being irradiated for 500 ms with the decoupler channel. After an exponential line broadening of 10 Hz was applied, the free induction decays (FIDs) were subtracted and Fourier transformed to obtain the NOE difference spectra.

For the NOESY spectra in H_2O buffer, the pulse sequence used was (delay–90°–t_1–90°–t_m–1331–acquire)$_n$, followed by FID collection. The time-proportional phase increment (TPPI) algorithm was used to obtain a phase-sensitive mode (Bodenhausen et al., 1984). The last 90° detection pulse was replaced by a 1331 pulse to suppress the H_2O signal (Hore, 1983). A total of 512 t_1 spectra was collected and processed by a 2K × 2K 2D Fourier transformation. A total of 320 scans was accumulated in each t_1 dimension. Two dummy scans were used. The sweep width was 11 111 Hz. The recycle delay and mixing time were 1.2 s and 200 ms, respectively. The spectra were phase-cycled with a 20% variation in the mixing time to suppress zero-quantum peaks. The FIDs were subjected to trapezoidal apodization using TM1 = 50 and TM2 = 250 parameters in both dimensions before Fourier transformation. The digital resolution was 10.9 Hz/point in each dimension.

The NOESY spectra in D_2O buffer were recorded using the TPPI method, with mixing times of either 80, 100, or 300 ms. A total of 512 t_1 spectra was collected and processed by a 2K × 2K 2D Fourier transformation. A total of 96 and 240 scans was accumulated in each t_1 dimension for the unmodified and ABP-modified 15-mer duplexes, respectively. Two dummy scans were used. The sweep width was 4902 Hz. The recycle delay was 1.2 s. The data were apodized with a shifted ($\pi/3$) squared sine bell apodization function for the t_2 dimension and an unshifted sine bell apodization function for the t_1 dimension before Fourier transformation. The digital resolution was 4.4 Hz/point in both dimensions. The residual HDO resonance was weakly presaturated.

The COSY experiments in D_2O buffer were acquired in the magnitude mode (Aue et al., 1976). A total of 512 t_1 experiments was collected and processed by a 2K × 1K 2D Fourier transformation. The data were apodized with an unshifted sine bell window function in both dimensions before Fourier transformation.

RESULTS

The sequential numbering scheme for the unmodified 15-mer duplex is shown in Chart I. The sequences labeled from T1 to T15 and from A16 to A30 are the noncoding and coding strands, respectively. In the ABP-modified 15-mer duplex, the C8 position of the single guanosine (G11, shadowed) in the noncoding strand was covalently adducted to produce dG-C8-ABP, whose structure and numbering system are shown in Chart II. In order to address the structural consequences of this modification, we will initially focus on a detailed NMR spectral analysis of the unmodified 15-mer duplex and then conduct a comparative study on its ABP-modified analogue.

Chart I: Sequential Numbering Scheme of the 15-mer DNA Duplex

5'- T1 A2 C3 T4 C5 T6 T7 C8 T9 T10 G11 A12 C13 C14 T15 -3'
3'- A30 T29 G28 A27 G26 A25 A24 G23 A22 A21 C20 T19 G18 G17 A16 -5'

Chart II: Structure of *N*-(deoxyguanosin-8-yl)-4-aminobiphenyl (dG-C8-ABP)

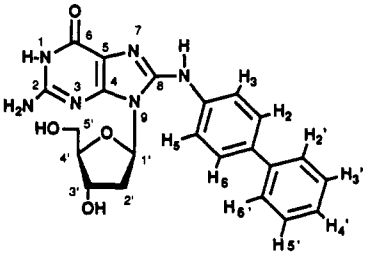

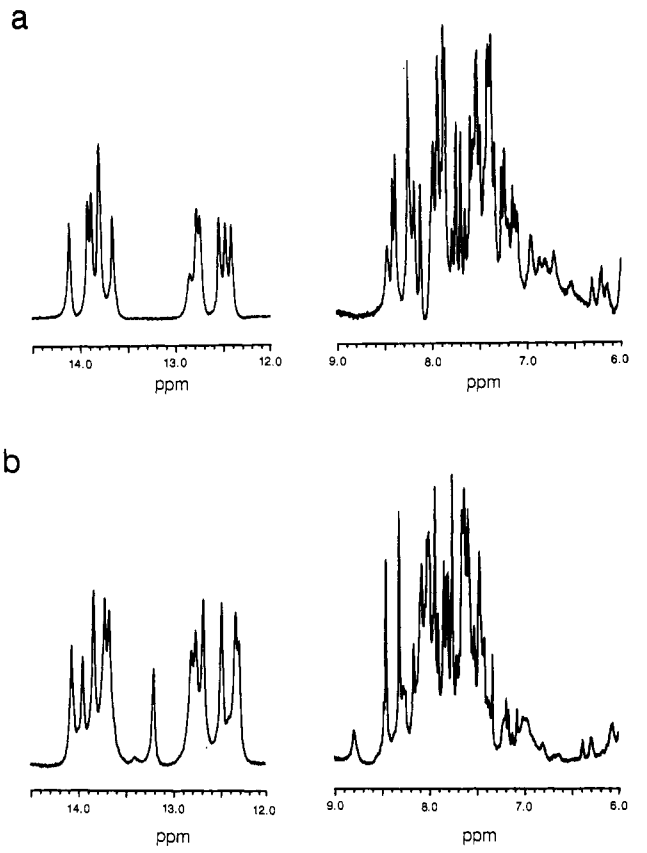

FIGURE 1: 1D 500-MHz proton NMR spectra of (a) the unmodified 15-mer duplex and (b) the ABP-modified 15-mer duplex in 90% H_2O/10% D_2O containing 100 mM NaCl, 10 mM sodium phosphate, and 100 μM disodium EDTA, pH 7.0 (H_2O buffer), at 14 °C.

Unmodified 15-mer Duplex

Assignment of the Exchangeable Protons. The imino and aromatic regions (12.0–14.5 and 6.0–9.0 ppm, respectively) of the 1D proton NMR spectrum of the unmodified 15-mer duplex, recorded in H_2O buffer at 14 °C, are plotted in Figure 1a. Eleven partially resolved imino proton resonances were observed in the range of 12.0–14.5 ppm. These resonances have been assigned primarily through the combined analysis of a 200-ms NOESY spectrum (Figure 2a) and 1D temperature-dependent proton spectra (Figure 3a), recorded in H_2O buffer [Boelens et al., 1985; for general procedures, see Wüthrich (1986) and references cited therein].

Three regions of the expanded NOESY contour plots, recorded in H_2O buffer at 5 °C, are shown in Figure 2a. They establish the NOE connectivities of each imino proton to its own or neighboring thymidine methyl protons (1.0–2.0 ppm, region I), to the opposite or adjacent cytidine amino and adenosine H2 protons (4.5–9.0 ppm, region II), and to its neighboring imino protons (symmetrical 12.0–14.5 ppm range, region III). Assignments of the numerically labeled NOE cross peaks in Figure 2a are listed in the figure legend, and the corresponding chemical shifts are given in Table I. In general terms, NOE peak patterns fully consistent with

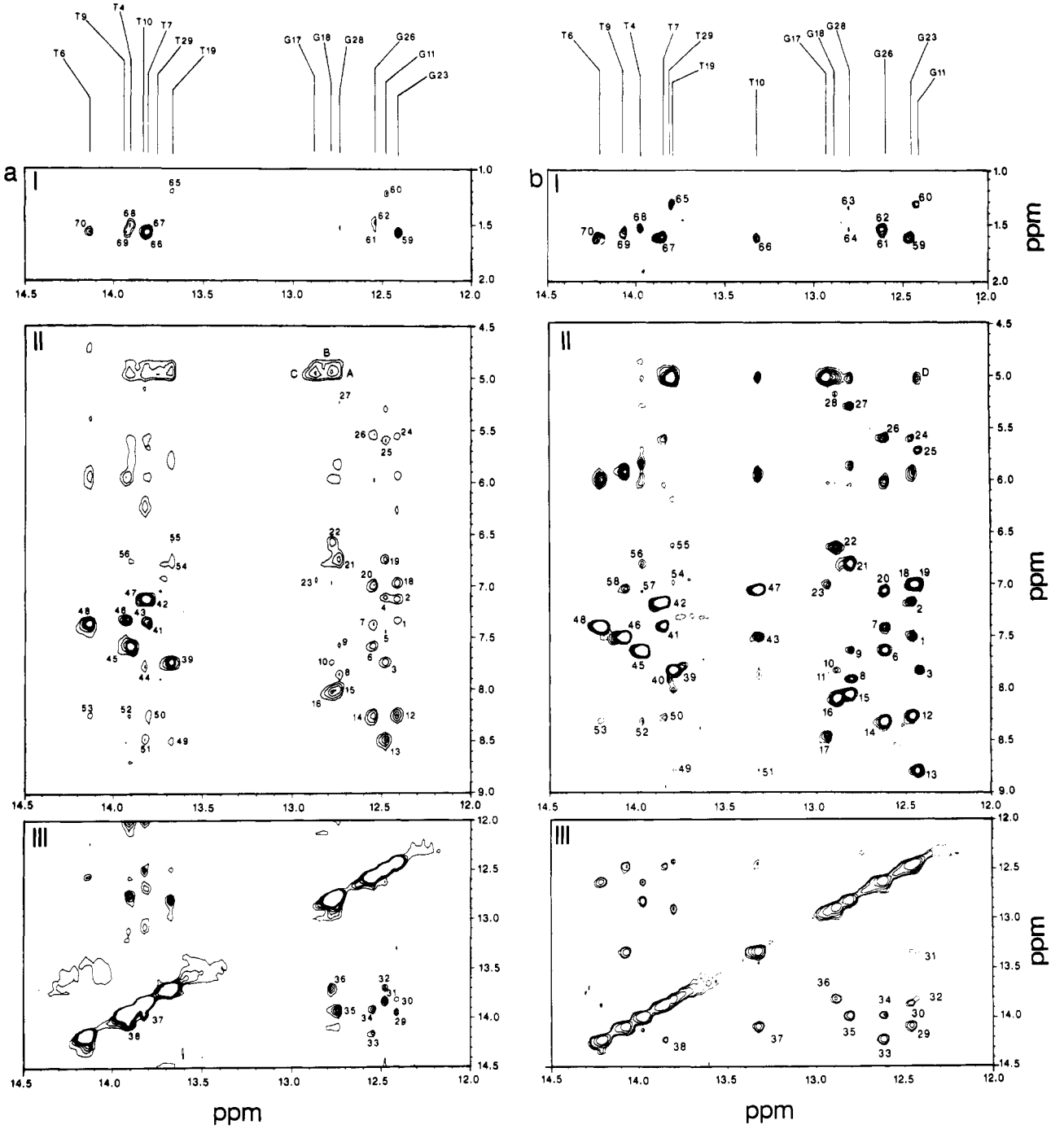

FIGURE 2: Expanded phase-sensitive NOESY contour plots (mixing time 200 ms) of (a) the unmodified 15-mer duplex and (b) the ABP-modified 15-mer duplex, in H_2O buffer at 5 °C. Cross peaks establish connectivities between imino protons (12.0–14.5 ppm) and thymidine methyl protons (1.0–2.0 ppm, region I), base and amino protons (4.5–9.0 ppm, region II), and neighboring imino protons (region III). The labeled cross peaks are assigned as follows: 1, G23(NH)–A22(H2); 2, G23(NH)–A24(H2); 3, G11(NH)–A12(H2); 4, G11(NH)–A21(H2); 5, G11(NH)–C20(H6); 6, G26(NH)–A27(H2); 7, G26(NH)–A25(H2); 8, G28(NH)–A2(H2); 9, G28(NH)–A27(H2); 10, G18(NH)–A12(H2); 11, G17(NH)–A16(H2); 12, G23(NH)–C8(NHb); 13, G11(NH)–C20(NHb); 14, G26(NH)–C5(NHb); 15, G28(NH)–C3(NHb); 16, G18(NH)–C13(NHb); 17, G17(NH)–C14(NHb); 18, G23(NH)–C8(NHe); 19, G11(NH)–C20(NHe); 20, G26(NH)–C5(NHe); 21, G28(NH)–C3(NHe); 22, G18(NH)–C13(NHe); 23, G17(NH)–C14(NHe); 24, G23(NH)–C8(H5); 25, G11(NH)–C20(H5); 26, G26(NH)–C5(H5); 27, G28(NH)–C3(H5); 28, G18(NH)–C13(H5); 29, G23(NH)–T9(NH); 30, G23(NH)–T7(NH); 31, G11(NH)–T10(NH); 32, G11(NH)–T19(NH); 33, G26(NH)–T6(NH); 34, G26(NH)–T4(NH); 35, G28(NH)–T4(NH); 36, G18(NH)–T19(NH); 37, T10(NH)–T9(NH); 38, T7(NH)–T6(NH); 39, T19(NH)–A12(H2); 40, T29(NH)–A2(H2); 41, T7(NH)–A25(H2); 42, T7(NH)–A24(H2); 43, T10(NH)–A22(H2); 44, T1(NH)–A30(H2) or T15(NH)–A16(H2); 45, T4(NH)–A27(H2); 46, T9(NH)–A22(H2); 47, T10(NH)–A21(H2); 48, T6(NH)–A25(H2); 49, T19(NH)–C20(NHb); 50, T7(NH)–C8(NHb); 51, T10(NH)–C20(NHb); 52, T4(NH)–C5(NHb); 53, T6(NH)–C5(NHb); 54, T19(NH)–C20(NHe); 55, T19(NH)–C13(NHe); 56, T4(NH)–C3(NHe); 57, T4(NH)–C5(NHe); 58, T9(NH)–C8(NHe); 59, G23(NH)–T7(Me)/G23(NH)–T9(Me); 60, G11(NH)–T19(Me); 61, G26(NH)–T6(Me); 62, G26(NH)–T4(Me); 63, G28(NH)–T29(Me); 64, G28(NH)–T4(Me); 65, T19(NH)–T19(Me); 66, T10(NH)–T10(Me); 67, T7(NH)–T7(Me); 68, T4(NH)–T4(Me); 69, T9(NH)–T9(Me); and 70, T6(NH)–T6(Me); A, G28(NH)–H_2O; B, G18(NH)–H_2O; C, G17(NH)–H_2O; D, G11(NH)–H_2O.

Watson–Crick base pair formation were detected for all the imino protons, with the exception of those belonging to the frayed terminal base pairs.

The initial step used in assigning the exchangeable protons of the unmodified duplex was the identification of the six expected guanosine imino protons in the range of 12.0–13.0

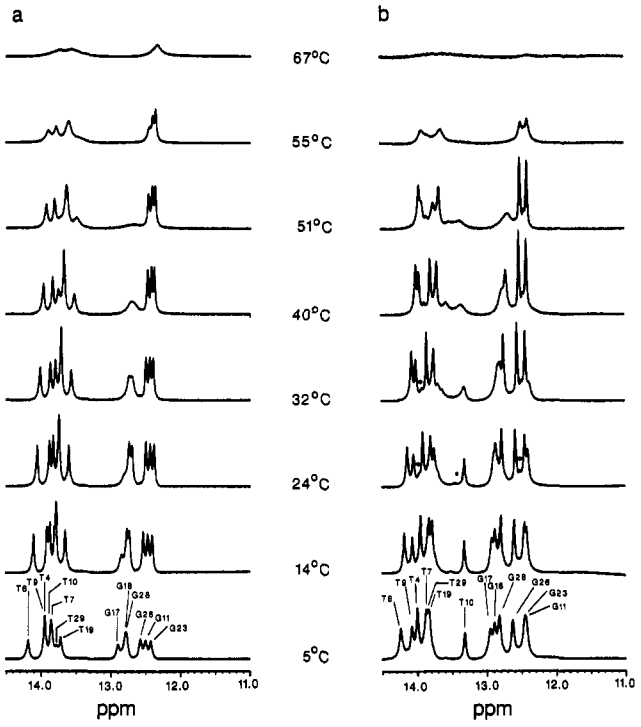

FIGURE 3: 1D proton NMR spectra of (a) the unmodified 15-mer duplex and (b) the ABP-modified 15-mer duplex in H_2O buffer, representing the temperature-dependent variations in the imino proton region (11.0–14.5 ppm). Peaks marked with asterisks in the spectra of the ABP-modified 15-mer duplex are due to the imino protons of the minor conformations, which are in slow exchange with the major conformer (see text).

ppm. Four of the six imino protons, arising from the internal G:C base pairs (i.e., G11:C20, G23:C8, G26:C5, and G28:C3), were readily identified since they developed weak NOEs to the cytidine H5 protons within each individual G:C pair (peaks 24–27, Figure 2a-II). An additional weak NOE was detected at 7.51 ppm (peak 5, Figure 2a-II), stemming from the interaction between the imino proton of G11 [G11(NH)] and the H6 proton of C20 within the G11:C20 pair, presumably due to a spin diffusion effect. The assignment of these H5 and H6 cytidine protons (vide infra) was readily obtained from analyses of the COSY (not shown) and NOESY spectra (Figure 4a), recorded in D_2O buffer. Furthermore, the imino protons of the internal guanosines exhibited strong NOEs to the hydrogen-bonded [C(NHb)] (peaks 12–15, Figure 2a-II) and exposed [C(NHe)] (peaks 18–21, Figure 2a-II) cytidine amino protons within individual G:C pairs, as well as to the nonexchangeable adenosine H2 protons [A(H2)] (peaks 1–4 and 6–9, Figure 2a-II) in the neighboring A:T pairs. For each individual cytidine, both amino protons were found to be NOE connected to the H5 proton, as well as to each other (not shown).

Of the two yet unidentified guanosine imino proton resonances, the one at 12.82 ppm was assigned to the G18:C13 pair, since a weak NOE to the H2 proton of A12 (peak 10, Figure 2a-II) was detected. Moderately intense cross peaks to the hydrogen-bonded and exposed amino protons of C13 (peaks 16 and 22, respectively, Figure 2a-II) supported this assignment. The remaining guanosine resonance at 12.91 ppm, exhibiting fast broadening even in the low temperature range (e.g., 5–14 °C, Figure 3a), was then assigned to the nearly terminal G17:C14 base pair, for which the strong attenuation of otherwise predictable NOEs (e.g., peak 23, Figure 2a-II) could be attributed to fraying of the oligonucleotide ends. In addition, it should be noted that while the imino protons of the three most internal G:C base pairs, G11:C20, G23:C8, and G26:C5, did not exhibit exchange cross peaks to the H_2O resonance, approximately at 5.0 ppm (Figure 2a-II), those in the nearly terminal G:C base pairs, G28:C3, G18:C13, and G17:C14, showed strong exchange cross peaks to the H_2O resonance (peaks A, B, and C, respectively, Figure 2a-II), an observation consistent with significant solvent exposure of these protons. The weak NOEs to the adenosine H2 protons of the neighboring A:T base pairs observed for the G18 (peak 10) and G28 (peaks 8 and 9, Figure 2a-II) imino protons further substantiated the occurrence of terminal fraying.

On the basis of the assignments of the guanosine imino protons discussed above, we could readily identify the thymidine imino protons, which resonated in the range of 13.5–14.5 ppm. The six thymidine imino proton resonances arising from the internal A:T base pairs (i.e., A27:T4, A25:T6, A24:T7, A22:T9, A21:T10, and A12:T19) exhibited strong NOEs to the adenosine H2 protons within individual (peaks 39, 42, and 45–48, Figure 2a-II) and neighboring (peaks 41 and 43, Figure 2a-II) A:T base pairs. Weak NOEs were also detected between some of these thymidine imino protons and the hydrogen-bonded (peaks 49–53, Figure 2a-II) and exposed (peaks 54–56, Figure 2a-II) cytidine amino protons in their adjacent G:C base pairs. It is noteworthy that the imino proton of the nearly terminal A2:T29 base pair was only detected at the lower temperature range (e.g., 5 °C, Figure 3a), due to terminal fraying, and gave a very weak NOE to the H2 proton of A2, which could only be detected at a higher contour level. We were unable to identify the imino protons of the terminal T1 and T15, which were presumably too broad to be detected even at low temperature. A weak cross peak at 7.78 ppm (peak 44, Figure 2a-II) could be assigned to the H2 proton of either A16 or A30.

The nonterminal imino proton assignments were further confirmed by tracing the imino–imino proton connectivities between flanking A:T and G:C base pairs (Figure 2a-III). Specifically, the imino proton of T4 exhibited an NOE to the G28 imino proton (peak 35, Figure 2a-III) of the adjacent G28:C3 pair in one direction and to the G26 imino proton (peak 34, Figure 2a-III) of the adjacent G26:C5 pair in the other direction, while the G26 imino proton in turn displayed an NOE (peak 33, Figure 2a-III) to the T6 imino proton in its flanking A25:T6 pair. In a similar manner, the G23 imino proton developed NOEs to the T9 and T7 imino protons in A22:T9 and A24:T7 (peaks 29 and 30, respectively). Analogous connections could be made between the G11 imino proton and the T10 and T19 imino protons (peaks 31 and 32, respectively) in A21:T10 and A12:T19, while another NOE (peak 36, Figure 2a-III) was observed between the imino protons of G18 and T19. Additional weak NOEs, which could be detected at a higher contour level, traced the interactions between thymidine imino protons, T6–T7 and T9–T10, in adjacent A:T base pairs (peaks 38 and 37, respectively).

Box I of Figure 2a shows weak to medium NOE cross peaks between the nonterminal imino protons and their own (peaks 65–70) and adjacent (peaks 59–62) thymidine methyl protons, which provided a further confirmation of the imino proton assignments. Independent assignments of the thymidine methyl resonances were obtained from analyses of intranucleotide long-range COSY and intrastrand NOE connectivities in the NOESY spectra recorded in D_2O buffer (not shown).

Several remaining unassigned cross peaks in the 5.5–6.5 ppm range (Figure 2a-II) were assumed to arise either from the interactions between imino protons and adenosine and/or

Table I: Comparison of Proton Chemical Shifts of the Unmodified and the ABP-Modified 15-mer Duplexes in H_2O Buffer[a]

	T(NH)/G(NH)			C(NHb)[b]			C(NHe)[c]			A(H2)		
base pair	15-mer	ABP 15-mer	Δδ[d]	15-mer	ABP 15-mer	Δδ	15-mer	ABP 15-mer	Δδ	15-mer	ABP 15-mer	Δδ
T1–A30	ND[e]	ND								ND	ND	
A2–T29	13.76	13.82	–0.06							7.87	7.92	–0.05
C3–G28	12.78	12.80	–0.02	8.05	8.07	–0.02	6.79	6.81	–0.02			
T4–A27	13.95	13.97	–0.02							7.58	7.65	–0.07
C5–G26	12.58	12.63	–0.05	8.29	8.31	–0.02	7.07	7.05	+0.02			
T6–A25	14.17	14.21	–0.04							7.48	7.42	+0.06
T7–A24	13.84	13.84	0.00							7.12	7.18	–0.06
C8–G23	12.45	12.45	0.00	8.29	8.29	0.00	7.03	7.05	–0.02			
T9–A22	13.97	14.06	–0.09							7.33	7.50	**–0.17**
T10–A21	13.86	13.32	**+0.54**							7.10	7.05	+0.05
G11–C20	12.52	12.43	+0.09	8.53	8.79	**–0.26**	6.79	6.99	**–0.20**			
A12–T19	13.71	13.80	–0.09							7.73	7.85	**–0.12**
C13–G18	12.82	12.89	–0.07	8.07	8.11	–0.04	6.62	6.64	–0.02			
C14–G17	12.91	12.93	–0.02	8.44	8.44	0.00	6.99	7.05	–0.06			
T15–A16	ND	ND								ND	ND	

[a] Chemical shifts are reported in ppm downfield from TSP at 5 °C. Samples were dissolved in 90% H_2O/10% D_2O contg. 100 mM NaCl, 10 mM sodium phosphate, and 100 μM disodium EDTA (H_2O buffer), pH 7.0. [b] Hydrogen-bonded cytidine amino proton. [c] Exposed cytidine amino proton. [d] Δδ = δ (unmodified 15-mer) – δ (ABP-modified 15-mer), Δδ > 0.1 ppm are shown in boldface. – indicates downfield shift and + indicates upfield shift of protons in the ABP-modified 15-mer duplex. [e] ND, not detected.

guanosine amino protons, or from NOEs involving guanosine imino protons and interstrand sugar H1′ protons. It has been shown that the flipping rates of adenosine amino protons are slower than those of guanosine in this temperature range (Fazakerley et al., 1984).

Finally, analysis of the temperature-dependent line broadening pattern of specific imino resonances (Figure 3a) confirmed the expected relative labilities of these protons. This broadening, due to solvent exchange, proceeded in an orderly manner upon raising the temperature, from the imino proton of the nearly terminal G17:C14 base pair at 24 °C to the imino proton resonances assigned to the G18:C13, G28:C3, A12:T19, and A27:T4 base pairs, and proceeding to those of the internal base pairs, which broadened above 51 °C. The observation that the terminal or nearly terminal imino protons were frayed and thereby exhibited strong cross peaks to the H_2O resonance in the NOESY spectrum taken in H_2O buffer (Figure 2a-II) was totally consistent with these results.

Assignment of the Nonexchangeable Protons. Many of the nonexchangeable protons of the unmodified 15-mer duplex were assigned through analyses of the NOESY and COSY spectra recorded in D_2O buffer. Our observations were fully compatible with the use of well-established rules [Hare et al., 1983; Feigon et al., 1983; see Wüthrich (1986) for a general procedure], based on the proximity of the sugar H1′, H2′, H2″, and H3′ protons to the base protons on the same and on the 3′-adjacent residues, in a typical B-DNA conformation.

Figure 4a shows, in duplicate, a portion of a 300-ms NOESY spectrum, recorded in D_2O buffer at 27 °C, displaying the interactions between the base H8/H6 protons (7.0–8.5 ppm) and the sugar H1′ and base H5 protons (5.0–6.5 ppm). The cross peaks between cytidine H5 and H6 protons were readily identified by their presence in the COSY spectrum (not shown) and are denoted by boldface characters (e.g., **C3**, **C13**, **C20**, and **C′**; see the figure legend).

Starting from the H6 proton (7.28 ppm) of the 5′-terminal T1 residue in the noncoding strand, the connectivities could be sequentially traced to reach the sugar H1′ proton (6.26 ppm) of T15 (Figure 4a-I). In general, the cross peaks were well separated, although the T1(H1′)–A2(H8) NOE interaction was very weak due to terminal fraying, and the cross peaks arising from the internal C5–T6–T7–C8 segment were not well resolved from one another. In most cases, potential ambiguities in the sequential tracing were solved by analyzing NOE connectivities in other regions of the NOESY spectrum. In a similar manner, the NOE tracing for the coding strand could be followed from A16 to A30 without ambiguity (Figure 4a-II). The sequential intrastrand interactions thus obtained are linked by continuous solid lines in Figure 4a. Also shown in Figure 4a are several minor inter- and intraresidue cross peaks, which are identified in the figure legend.

In addition to the resonance assignments, the analysis of Figure 4a suggested that intraresidue NOE interactions between base H8/H6 and sugar H1′ protons (e.g., C3 and C13) were weaker than those detected between cytidine H5 and H6 protons (e.g., **C3** and **C13**). This observation was further substantiated by recording a NOESY spectrum in D_2O buffer, using a shorter mixing time (100 ms). These results indicated that the H8/H6 to H1′ distances were longer than the fixed length (~2.4 Å) between the H5 and H6 protons of cytidine, establishing that each base residue adopted an anti conformation about its glycosyl bond (Patel et al., 1982).

As a consequence of their long spin–lattice relaxation time values, all the nine expected minor groove adenosine H2 protons were readily distinguished from the other nonexchangeable base protons by 1D inversion–recovery experiments (not shown) performed in D_2O buffer at 27 °C. The seven H2 protons of the nonterminal adenosines have been previously assigned (vide supra) on the basis of their NOEs to guanosine and thymidine imino protons in the NOESY spectrum recorded in H_2O buffer (Figure 2a-II and Table I). The remaining adenosine H2 resonances, observed at 7.78 and 7.92 ppm in the D_2O spectrum, could be assigned to either A16 or A30 in the terminal base pairs. It should be noted that the chemical shift values of the adenosine H2 protons obtained in D_2O buffer (Table II) were slightly different (≤0.09 ppm) from those observed in H_2O buffer (Table I), presumably due to a combination of solvent and temperature effects.

The sugar protons were assigned by a combined analysis of the COSY and 100-ms NOESY spectra. The H2′ and H2″ resonances were distinguished from one another by the greater intensity of the H2″–H1′ NOESY cross peaks, while the H3′ resonances were confirmed on the basis of the H2′/H2″–H3′ connectivities. For all of the nucleotides, the H2′ proton resonated upfield from H2″ (Table II), with the exception of the 3′-terminal residues, where either the H2′ and H2″ resonances had identical chemical shifts (e.g., T15) or the

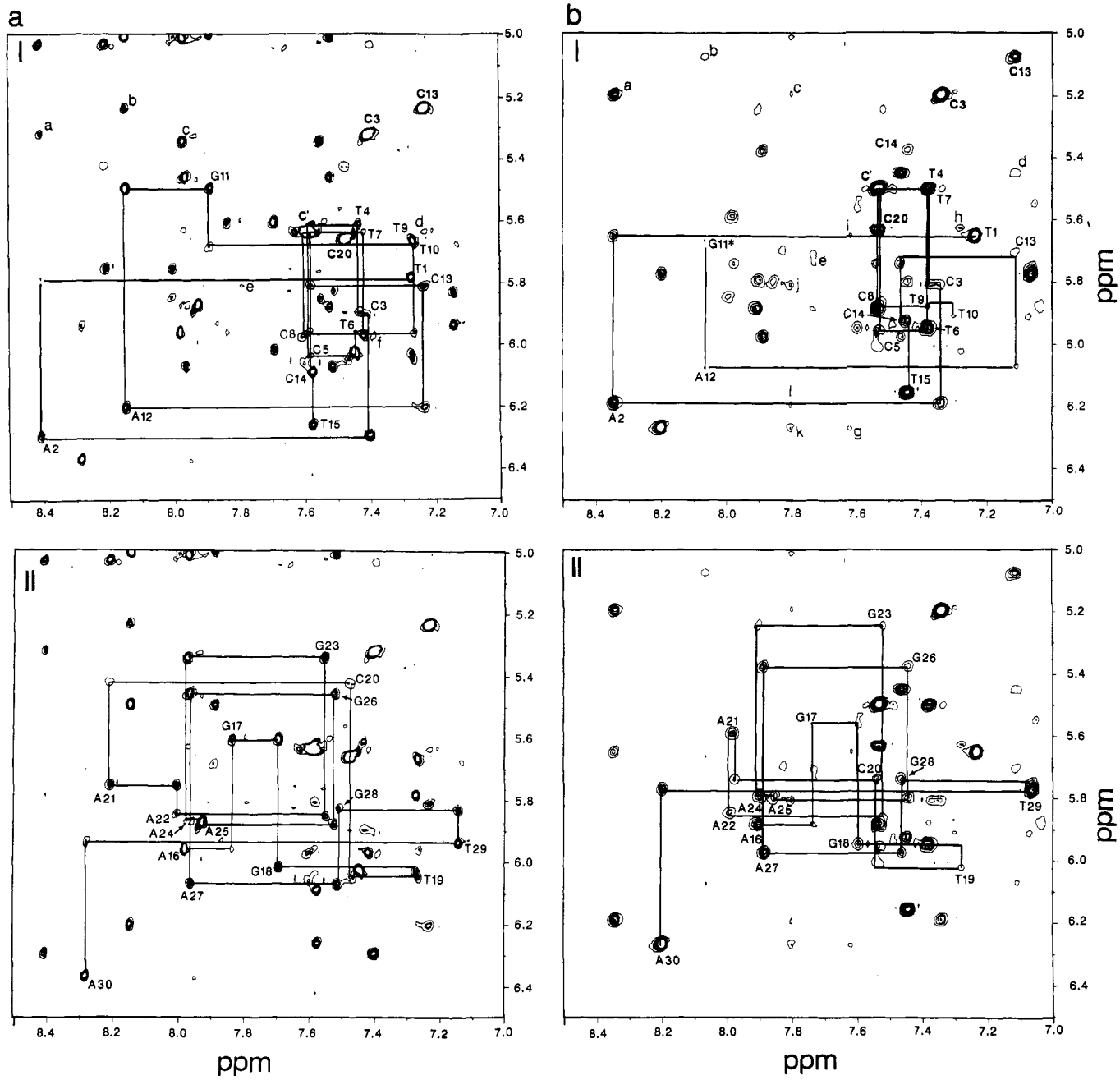

FIGURE 4: Expanded phase-sensitive NOESY contour plots (mixing time 300 ms) of (a) the unmodified 15-mer duplex at 27 °C and (b) the ABP-modified 15-mer duplex at 5 °C, both taken in D_2O containing 100 mM NaCl, 10 mM sodium phosphate, and 100 μM disodium EDTA, pH 7.0 (D_2O buffer), establishing connectivities between the base H6/H8 protons (7.0–8.5 ppm) and the sugar H1′ and cytidine H5 protons (5.0–6.5 ppm). The solid lines trace sequential distance connectivities between the base and the sugar protons in the noncoding and coding strands (plots I and II, respectively). With the exception of G11*(H1′)–A12(H8) in the ABP-modified duplex, cross peaks labeled by base and sequence position are due to intranucleotide interactions. Cross peaks due to cytidine H5–H6 connectivities are denoted by boldface characters (e.g., **C3**, **C13**, **C20**, and **C′**). **C′** represents overlapped C5, C8, and C14 signals in the plot of the unmodified duplex (Figure 4a) and overlapped C5 and C8 signals in the plot of the ABP-modified duplex (Figure 4b). The remaining cross peaks are assigned as follows: a, A2(H8)–C3(H5); b, A12(H8)–C13(H5); c, A2(H2)–C3(H5); d, C13(H6)–C14(H5); e, A12(H2)–C13(H1′); f, A22(H2)–C8(H1′); g, A30(H2)–A30(H1′); h, T19(H6)–C20(H5); i, A30(H2)–T1(H1′); j, A2(H2)–C3(H1′); k, A2(H2)–A30(H1′); and l, A2(H2)–A2(H1′).

order was reversed (e.g., A30). In addition, the H2′ resonance of the 5′-terminal T1 (1.60 ppm) was unusually shielded when compared to those (≥1.93 ppm) in the other nucleotides. Similarly, the H3′ sugar protons of the 3′-terminal residues (e.g., 4.56 and 4.70 ppm, respectively, for T15 and A30) resonated at higher field than the same H3′ protons of other T or A nucleotides, mainly due to lack of the ring-current effect for the 3′-terminal bases (Table II). The H4′ and H5′ protons were not assigned except for the 5′-protons of the 5′-terminal T1 and A16 residues that were uniquely shielded, resonating at 3.62 and 3.68 ppm, respectively, due to the absence of the 5′-phosphorylated functional group.

ABP-Modified 15-mer Duplex

Figure 1b shows the imino and aromatic proton regions (12.0–14.5 and 6.0–9.0 ppm, respectively) of the 1D proton spectrum for the ABP-modified 15-mer duplex, recorded in H_2O buffer at 14 °C. A total of 12 resolvable imino proton resonances was observed in the downfield region (12.0–14.5 ppm). One isolated resonance was noted at 13.32 ppm, in the range consistent with thymidine imino protons, but shielded

Table II: Comparison of the Proton Chemical Shifts of the Unmodified and the ABP-Modified 15-mer Duplexes in D_2O Buffer[a]

	H8/H6			H5/CH3			H1′			H2′			H2″			H3′			H2[c]		
base	15-mer	ABP 15-mer	Δδ[b]	15-mer	ABP 15-mer	Δδ	15-mer	ABP 15-mer	Δδ	15-mer	ABP 15-mer	Δδ	15-mer	ABP 15-mer	Δδ	15-mer	ABP 15-mer	Δδ	15-mer	ABP 15-mer	Δδ
T1	7.28	7.23	+0.05	1.58	1.50	+0.08	5.79	5.65	**+0.14**	1.60	1.59	+0.01	2.18	2.11	+0.07	4.62	4.55	+0.07			
A2	8.41	8.35	+0.06				6.29	6.19	+0.10	2.86	2.78	+0.08	2.93	2.86	+0.07	5.02	4.96	+0.06	7.94	7.80	**+0.14**
C3	7.40	7.34	+0.06	5.32	5.20	**+0.12**	5.90	5.80	+0.10	2.05	1.98	+0.07	2.55	2.47	+0.08	4.63	4.53	+0.10			
T4	7.44	7.37	+0.07	1.54	1.45	+0.09	5.62	5.50	**+0.12**	2.26	2.10	**+0.16**	2.57	2.44	**+0.13**	4.87	4.70	**+0.17**			
C5	7.57	7.53	+0.04	5.61	5.50	**+0.11**	6.04	5.96	+0.08	2.24	NA[d]		2.50	NA		4.88	NA				
T6	7.44	7.39	+0.05	1.62	1.53	+0.09	5.96	5.93	+0.03	2.12	NA		2.51	NA		4.86	NA				
T7	7.42	7.38	+0.04	1.64	1.53	**+0.11**	5.63	5.50	**+0.13**	2.10	NA		2.49	NA		4.85	NA				
C8	7.61	7.54	+0.07	5.65	5.50	**+0.15**	5.95	5.88	+0.07	2.15	NA		2.51	NA		4.90	NA				
T9	7.27	7.38	**−0.11**	1.62	1.52	+0.10	5.66	5.87	**−0.21**	1.97	NA		2.33	NA		4.84	NA				
T10	7.26	7.31	−0.05	1.66	1.53	**+0.13**	5.68	5.91	**−0.23**	1.96	NA		2.34	NA		4.85	NA				
G11	7.88						5.49	5.67	**−0.18**	2.69	NA		2.76	NA		5.00	NA				
A12	8.15	8.07	+0.08				6.20	6.08	**+0.12**	2.66	2.53	**+0.13**	2.87	2.77	+0.10	5.01	NA		7.77	7.73	+0.04
C13	7.24	7.11	**+0.13**	5.24	5.08	**+0.16**	5.81	5.71	+0.10	1.98	1.91	+0.07	2.38	2.32	+0.06	4.83	4.68	**+0.15**			
C14	7.57	7.45	**+0.12**	5.65	5.45	**+0.20**	6.09	5.93	**+0.16**	2.26	2.10	**+0.16**	2.48	2.39	+0.09	4.82	4.69	**+0.13**			
T15	7.57	7.44	**+0.13**	1.75	1.58	**+0.17**	6.26	6.16	+0.10	2.30	2.21	+0.09	2.30	2.21	+0.09	4.56	4.48	+0.08			
A16	7.98	7.91	+0.07				5.96	5.89	+0.07	2.40	2.44	−0.04	2.51	2.58	−0.07	4.85	4.75	+0.10	7.78[e]	7.69	
G17	7.83	7.73	+0.10				5.60	5.57	+0.03	2.53	2.52	+0.01	2.65	2.65	0.00	4.82	4.87	−0.05			
G18	7.70	7.60	+0.10				6.01	5.95	+0.06	2.57	2.50	+0.07	2.79	2.69	+0.10	4.90	4.79	**+0.11**			
T19	7.27	7.28	−0.01	1.30	1.23	+0.07	6.05	6.02	+0.03	2.10	2.12	−0.02	2.49	2.57	−0.08	4.90	4.80	+0.10			
C20	7.47	7.53	−0.06	5.66	5.62	+0.04	5.42	5.74	**−0.32**	1.94	NA		2.28	NA		4.82	NA				
A21	8.21	7.98	**+0.23**				5.75	5.59	**+0.16**	2.72	2.42	**+0.30**	2.82	2.61	**+0.21**	5.03	4.92	**+0.11**	7.17	6.96	**+0.21**
A22	8.01	7.99	+0.02				5.84	5.85	−0.01	2.54	2.53	+0.01	2.76	2.74	+0.02	5.01	4.96	+0.05	7.38	7.42	−0.04
G23	7.55	7.52	+0.03				5.33	5.24	+0.09	2.42	2.38	+0.04	2.59	2.53	+0.06	4.94	4.87	+0.07			
A24	7.97	7.90	+0.07				5.87	5.79	+0.08	2.53	2.46	+0.07	2.82	2.73	+0.09	5.01	4.93	+0.08	7.21	7.07	**+0.14**
A25	7.94	7.86	+0.08				5.88	5.80	+0.08	2.53	2.47	+0.06	2.79	2.73	+0.06	5.01	4.94	+0.07	7.42	7.30	**+0.12**
G26	7.52	7.44	+0.08				5.46	5.38	+0.08	2.45	2.36	+0.09	2.65	2.57	+0.08	4.94	4.87	+0.07			
A27	7.96	7.89	+0.07				6.07	5.98	+0.09	2.61	2.53	+0.08	2.86	2.78	+0.08	4.94	4.93	+0.01	7.64	7.54	+0.10
G28	7.51	7.46	+0.05				5.82	5.75	+0.07	2.37	2.30	+0.07	2.59	2.53	+0.06	4.89	4.82	+0.07			
T29	7.15	7.06	+0.09	1.37	1.26	+0.09	5.94	5.78	**+0.16**	1.93	1.84	+0.09	2.25	2.17	+0.08	4.74	4.70	+0.04			
A30	8.28	8.20	+0.08				6.36	6.27	+0.09	2.75	2.70	+0.05	2.53	2.42	**+0.11**	4.70	4.63	+0.07	7.92[e]	7.62	

[a] Chemical shifts are reported in parts per million downfield from TSP. Samples were dissolved in D_2O containing 100 mM NaCl, 10 mM sodium phosphate, and 100 μM disodium EDTA (D_2O buffer), pH 7.0 The temperature was 27 °C for the unmodified duplex and 5 °C for the ABP-modified duplex. The H4′ and H5′ protons were not asigned, except for the H5′ methylene protons of the 5′-terminal T1 (3.62 and 3.55 ppm for the unmodified and ABP-modified 15-mers, respectively) and A16 (3.68 and 3.62 ppm, respectively) nucleotides. [b] $\Delta\delta = \delta$ (unmodified 15-mer) − δ (ABP-modified 15-mer); $\Delta\delta > 0.1$ ppm are shown in boldface. − indicates downfield shift and + indicates upfield shift of protons in the ABP-modified 15-mer duplex. [c] Obtained by 1D inversion–recovery experiments. [d] NA, not assigned due to weak or overlapped cross peaks. [e] Assignments may be interchanged.

in comparison to the remaining thymidine imino protons. In general, the peaks were well resolved and their line widths were comparable to those observed for the parent duplex, allowing a detailed 2D proton NMR study to be performed. However, in contrast with the unmodified duplex, additional minor resonances were detected in the proton spectra of the ABP-modified species (Figure 3b, vide infra), indicative of the presence of more than one conformation in slow equilibrium. The present study concentrates primarily on the structural characterization of the major conformation.

Assignment of the Exchangeable Nucleic Acid Protons. A 200-ms NOESY spectrum for the ABP-modified 15-mer duplex was recorded under the same experimental conditions (pH 7.0, H_2O buffer, 5 °C) that were used for the unmodified duplex. For the sake of comparison, three expanded regions, matching those in Figure 2a, are plotted in Figure 2b. The assignments of the imino proton resonances for the modified duplex were performed similarly as described for the unmodified duplex, through a combined analysis of NOESY and 1D temperature-dependent imino proton spectra. Additional confirmation of all the imino proton assignments was achieved by performing 1D NOE difference experiments (not shown). Whenever possible, the key NOE cross peaks are labeled with the same arabic numbers that were used for the corresponding cross peaks in the unmodified duplex (compare Figure 2 panels a and b). Some NOE connectivities observed in the unmodified 15-mer duplex (Figure 2a) may not be present in the modified duplex (Figure 2b) and vice versa, reflecting their differences in conformational structures. The assigned chemical shifts of the exchangeable (imino and amino) and of the adenosine H2 protons for the ABP-modified duplex are listed in Table I, along with the observed differences from their analogues in the parent duplex.

Despite the ABP modification, the interaction between most of the exchangeable protons and the solvent appeared to be slow, as reflected by the presence of well-shaped cross peaks between exchangeable and nonexchangeable protons and, even more convincingly, between pairs of exchangeable protons in the NOESY spectrum (Figure 2b). A comparison of Figure 2 panels a and b revealed striking similarities in the NOE cross peak patterns for the unmodified and ABP-modified oligomer duplexes.

As in the case of the unmodified duplex, the imino proton signals of the terminal base pairs were strongly attenuated, due to the terminal fraying effects. With the exception of the nearly terminal G17, the internal guanosine imino protons exhibited strong NOE cross peaks to the adenosine H2 protons in adjacent A:T base pairs (peaks 1–3 and 6–10, Figure 2b-II) and to the hydrogen-bonded (peaks 12–16, Figure 2b-II) and exposed (peaks 18–22, Figure 2b-II) cytidine amino protons within individual G:C base pairs. In addition, each of these guanosine imino protons also developed a weak to medium NOE to the H5 proton of its partner cytidine (peaks 24–28, Figure 2b-II). Independent assignment of these nonexchangeable cytidine H5 protons was obtained through analysis of the COSY and NOESY spectra recorded in D_2O buffer (vide infra). For each individual cytidine, the H5 and both amino protons were all found to be mutually NOE connected, as shown in the plot of the corresponding region (6.6–9.0 vs 4.5–9.0 ppm, Figure 5) of the NOESY spectrum

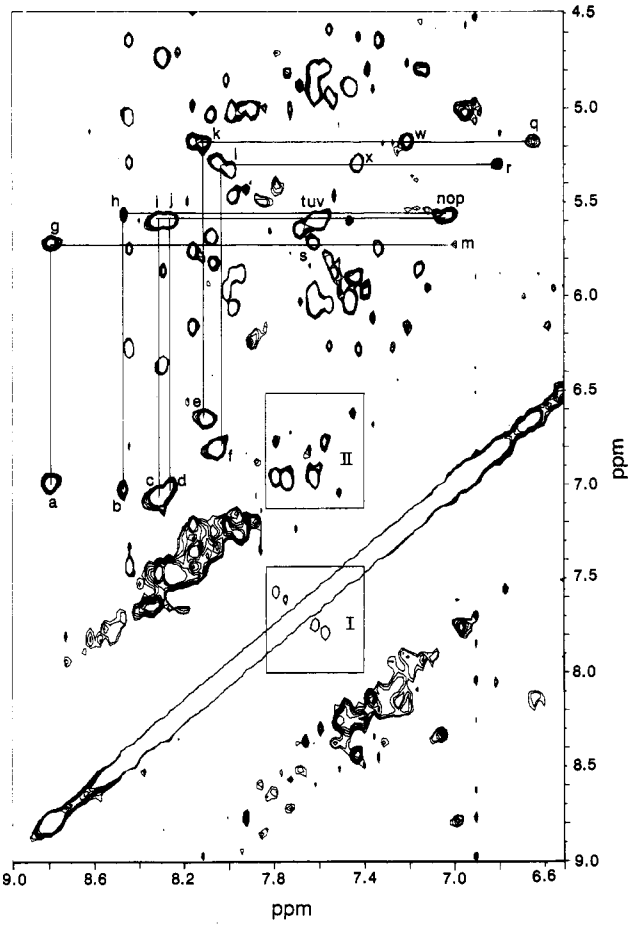

FIGURE 5: Expanded phase-sensitive NOESY contour plots (mixing time 200 ms) of the ABP-modified 15-mer duplex in H_2O buffer at 5 °C. The boxed regions I and II display the cross peaks related to the ABP ring protons of the major and minor conformers, respectively (see text). The labeled cross peaks are assigned as follows: a, C20(NHb)–C20(NHe); b, C14(NHb)–C14(NHe); c, C5(NHb)–C5(NHe); d, C8(NHb)–C8(NHe); e, C13(NHb)–C13(NHe); f, C3(NHb)–C3(NHe); g, C20(NHb)–C20(H5); h, C14(NHb)–C14(H5); i, C5(NHb)–C5(H5); j, C8(NHb)–C8(H5); k, C13(NHb)–C13(H5); l, C3(NHb)–C3(H5); m, C20(NHe)–C20(H5); n, C14(NHe)–C14(H5); o, C5(NHe)–C5(H5); p, C8(NHe)–C8(H5); q, C13(NHe)–C13(H5); r, C3(NHe)–C3(H5); s, C20(H6)–C20(H5); t, C14(H6)–C14(H5); u, C5(H6)–C5(H5); v, C8(H6)–C8(H5); w, C13(H6)–C13(H5); x, C3(H6)–C3(H5).

taken in H_2O buffer, where each set of mutually related cross peaks is linked by a solid line. Thus, for each cytidine, cross peaks were established between the hydrogen-bonded and exposed amino protons (peaks a–f, Figure 5), between the hydrogen-bonded amino and H5 protons (peaks g–l, Figure 5), and between the exposed amino and H5 protons (peaks m–q, Figure 5). Also observed were the cross peaks between the cytidine H5 and H6 protons (peaks s–x, Figure 5).

While the observation of cross peaks between the imino proton of G17 and both the hydrogen-bonded and exposed amino protons of C14 (peaks 17 and 23, respectively, Figure 2b-II) reflected the effective formation of a G17:C14 base pair, the presence of only a weak interaction with the H2 proton of A16 (peak 11, Figure 2b-II) was obviously due to terminal fraying. It should be noted that the measured differences in the chemical shifts of the hydrogen-bonded and exposed amino protons within each individual cytidine were comparable to the ones found for the unmodified duplex (Table I). This observation suggested that the base-pairing pattern of the parent duplex was retained in the ABP-modified species. However, both the hydrogen-bonded and exposed amino protons of C20, which was opposed to the [ABP]G11 adduct site in the modified duplex, were shifted downfield significantly (–0.26 and –0.20 ppm, respectively), when compared to the analogous protons in the parent duplex (Table I).

Identification of the imino protons corresponding to the six internal A:T base pairs followed readily from the above assignments, by means of tracing the flanking imino–imino proton connectivities from G18–T19 to T4–G28 (peaks 29–38, Figure 2b-III) throughout the 11 internal base pairs. The fact that there was no interruption in this tracing indicates that the ABP-modified oligomer duplex globally conserved the same type of stacking interactions that were observed in the unmodified duplex. In addition to their strong NOEs to the adenosine H2 protons within individual A:T base pairs (peaks 39, 42, and 45–48, Figure 2b-II), the internal thymidine imino protons also displayed weak to medium NOE cross peaks to both the hydrogen-bonded (peaks 49–53, Figure 2b-II) and exposed (peaks 54–58, Figure 2b-II) cytidine amino protons of adjacent G:C base pairs. For instance, the imino proton of T4, which was flanked by two cytidines, exhibited weak to medium NOEs to the hydrogen-bonded (peak 52, Figure 2b-II) and exposed (peaks 56 and 57, Figure 2b-II) amino protons of both C3 and C5, although its NOE to C3(NHb) could only be detected at a higher contour level. In addition, the imino protons of T7 and T10 developed NOEs to the adenosine H2 protons of the flanking A25:T6 and A22:T9 base pairs (peaks 41 and 43, respectively, Figure 2b-II). Although the imino protons of the two frayed terminal A:T base pairs were not detected, the remaining highly attenuated resonance at 13.82 ppm could be assigned to the imino proton of the nearly terminal T29, on the basis of a weak NOE to the H2 proton of its partner A2 (peak 40, Figure 2b-II).

The unique high-field imino proton resonance at 13.32 ppm appeared as a key characteristic of the ABP-modified 15-mer. It exhibited strong cross peaks to the H2 protons of A22 and A21 in the A22:T9 and A21:T10 base pairs (peaks 43 and 47, respectively, Figure 2b-II), as well as a weak NOE to the hydrogen-bonded amino proton of C20 (peak 51, Figure 2b-II), which opposed the ABP-modified G11. Therefore, the above resonance could be assigned unambiguously to the imino proton of T10, which was adjacent to the modification site in the 5′ direction.

Further corroboration of the above imino proton assignments could be obtained from the observation of the NOESY cross peaks stemming from interactions between thymidine methyl protons and the internal imino protons within individual A:T (peaks 65–70, Figure 2b-I) or adjacent G:C (peaks 59–64, Figure 2b-I) base pairs. The methyl signals for T6, T7, T9, and T10 were nearly degenerate (1.52–1.53 ppm, Table II). As discussed for the unmodified 15-mer, independent assignment of the methyl resonances was derived from the COSY and NOESY connectivities, obtained in D_2O buffer (not shown).

Assuming that the A21:T10, [ABP]G11:C20, and A12:T19 base pairs in the ABP-modified duplex maintained regular stacked Watson–Crick configurations, as detected in the unmodified duplex, the imino proton of [ABP]G11 would be expected to give NOEs to the H2 protons of the flanking A21 and A12 bases. Although the cross peak with A12(H2) was readily identified at 7.85 ppm (peak 3, Figure 2b-II), the presence of the cross peak with A21(H2) was not apparent, due to a possible overlap with the NOE cross peaks arising from the G23(NH)–C8(NHe) and G11(NH)–C20(NHe) interactions, approximately at 7.0 ppm (peaks 18 and 19, respectively, Figure 2b-II). We attempted to solve this

ambiguity by conducting 1D NOE difference experiments (not shown) but were not able to detect an unequivocal NOE to the H2 proton of the adjacent A21. This suggested that the regular stacking pattern of the parent duplex was disrupted between the A21:T10 and [ABP]G11:C20 base pairs. Nonetheless, the perturbation seems restricted to the immediate vicinity of the adduct site, with the overall NOE cross peak pattern virtually analogous to that observed in the parent duplex.

The most noticeable differences between the unmodified and modified duplexes were the upfield shifts detected for the imino protons of both T10 and [ABP]G11 in the ABP-modified 15-mer duplex, whereas the chemical shifts of the other imino protons were relatively unaffected as compared to the corresponding protons in the parent species (Table I). The magnitude of these shieldings was far greater for the imino proton of T10 (+0.54 ppm), which was located next to the modification site in the 5′ direction, than for the imino proton of the ABP-modified G11 (+0.09 ppm). In contrast, downfield shifts of comparable magnitude were observed for both the hydrogen-bonded and exposed (–0.26 and –0.20 ppm, respectively) amino protons of C20 in the [ABP]G11:C20 base pair. Similarly, the H2 protons of A22 and A12 in the A22:T9 and A12:T19 base pairs were deshielded by –0.17 and –0.12 ppm, respectively (Table I). It should also be noted that differences existed in the cross peaks between H_2O and the internal imino protons. For the unmodified duplex, the nearly terminal G:C base pairs (G28:C3, G18:C13, and G17:C14) showed strong exchange cross peaks to the H_2O resonance while the imino protons of the three most internal G:C base pairs (G11:C20, G23:C8, and G26:C5) did not (Figure 2a-II, vide supra). In the ABP-modified duplex, however, the imino proton of [ABP]G11:C20 exhibited a moderate exchange cross peak to the H_2O resonance (peak D, Figure 2b-II). This indicated that the site of modification had greater exposure to the solvent even though the duplex was largely intact. Although unlikely, the increased exchange of the [ABP]G11 imino proton may be due to a subtle change in its pK_a as a result of adduct formation.

The temperature dependence of the imino proton resonances in the ABP-modified duplex (Figure 3b) revealed a sequence of broadening somewhat different from the one observed for the unmodified parent duplex (Figure 3a). Thus, the imino proton of [ABP]G11 was as labile as those of the nearly terminal G17:C14 and G18:C13 base pairs. These were followed by those of the A21:T10 and A12:T19 base pairs that flanked the modification site. Subsequent broadening of the internal imino protons then occurred in a predictable manner as observed with the unmodified duplex. It is worth noting that the T10 imino proton of the ABP-modified 15-mer was deshielded upon raising the temperature, while all the other imino protons of both duplexes experienced steady upfield shifts under similar conditions. This unique behavior of the T10 imino proton could be attributed to a direct consequence of adduct formation at G11. From these and the results discussed above, substantial evidence exists that, although not disrupting duplex formation, the ABP moiety incorporated into G11 destabilizes the base pairs in the immediate vicinity of the modification site when compared to the analogous base pairs in the parent duplex.

In addition to these general conclusions, it should be stressed that the presence of several minor imino proton resonances (marked as asterisks) was clearly detected in Figure 3b, particularly in the spectra recorded at intermediate temperatures. Although these resonances remain unassigned, their existence indicated that at least one additional component exists in solution, in slow equilibrium with the major conformation of the ABP-modified duplex. The greater exposure of the [ABP]G11 imino proton to H_2O (e.g., peak D, Figure 2b-II) might be a consequence of the slow exchange between these conformations. These minor conformations will be discussed further in the following sections.

Assignment of the Nonexchangeable Nucleic Acid Protons. Initially, a NOESY spectrum of the ABP-modified 15-mer duplex was recorded in D_2O buffer at 27 °C, as was done for the unmodified 15-mer. It became immediately obvious that some NOE cross peaks, particularly those near the modification site (segments T9–T10 and G11–A12–C13) and at the fraying terminal bases, were either absent or too weak to be detected. This was not unexpected, since we have previously shown (Marques & Beland, 1990) that the melting temperature of the ABP-modified 15-mer duplex was substantially lower than that of the unmodified duplex. In order to detect the NOE cross peaks necessary for structural elucidation of the modification site, NOESY spectra were recorded at 20 and 5 °C. As expected, several more critical NOEs from nucleotides in the vicinity of the adduct were obtained at these lower temperatures.

For the reasons discussed above we will, in this section, focus on the analysis of the NOESY spectrum recorded at 5 °C. In general, the chemical shift variations for the nonexchangeable protons of the ABP-modified 15-mer duplex in this temperature range (5–27 °C) were almost negligible (<0.05 ppm). Exceptions existed for those of the bases located at or near the modification site and for those of the terminal bases, presumably due to a partial melting (vide infra). The chemical shift assignments obtained for the nonexchangeable base and most sugar protons of the ABP-modified duplex at 5 °C are given in Table II, in comparison with those of the parent duplex recorded at 27 °C.

Expanded portions outlining the sequential intrastrand NOE connectivities between the base H8/H6 protons (7.0–8.5 ppm) and the sugar H1′ and cytidine H5 protons (5.0–6.5 ppm) of a 300-ms NOESY spectrum recorded at 5 °C are shown in duplicate in Figure 4b. It should be mentioned that although some cross peaks in this figure appear unusually stronger than their counterparts in the parent duplex (Figure 4a), this can be attributed to temperature effects. Using the same principles applied to the unmodified duplex, the NOE connectivities in this region could be traced without any difficulties from the 5′-terminal A16 to the 3′-terminal A30 in the unmodified strand (Figure 4b-II). They could also be followed from T1 to T10 in the ABP-modified strand. The NOE interactions in the T9–T10 segment were too weak to be definitive, but potential ambiguities in the assignment of these cross peaks were solved by inspecting the NOE connectivities in other regions of the NOESY spectrum. No connection could be made from T10 to G11, which lacks the H8 proton as a result of covalent binding of the ABP moiety to the C8 position. The NOEs were resumed from the sugar H1′ of [ABP]G11 to the 3′-terminal A15. The sequential NOE connectivities are shown by solid lines in Figure 4 panels b-I and b-II; identical conventions were used for labeling the NOESY cross peaks of the unmodified and the ABP-modified 15-mer duplexes (Figure 4, panels a and b, respectively). Essentially the same type of sequential NOE connectivities could be traced in the corresponding region of the NOESY spectrum recorded in H_2O buffer (Figure 5). As observed for the unmodified duplex, the chemical shifts in the NOESY spectrum recorded in H_2O buffer (Figure 5) were consistently deshielded (ca. 0.1 ppm)

as compared to the values obtained in D_2O buffer (Figure 4b), which was attributed to solvent effects.

Four out of six possible interbase cross peaks corresponding to the interactions between the base H8/H6 protons and the H5 protons of 3′-flanking cytidines (peaks a, b, d, and h, Figure 4b) were detected for A2–C3, A12–C13, C13–C14, and T19–C20, respectively. Similar NOE interactions for T4–C5 and T7–C8, however, were not identified, presumably due to extensive overlapping in the corresponding region of the NOESY spectrum. Several weak to medium NOE interactions involving adenosine H2 protons were also detected and assigned (Figure 4b). In particular, the H2 proton of A2 developed multiple NOEs to the sugar H1′ protons of A2, A30, and C3 (peaks l, k, and j, respectively, Figure 4b-I) and to the H5 proton of C3 (peak c, Figure 4b-I). Similarly to those of the unmodified duplex, the sugar H5′ protons in the 5′-terminal nucleotides (e.g., 3.55 and 3.62 ppm for T1 and A16, respectively) and the sugar H3′ protons in the 3′-terminal nucleotides (e.g., 4.48 and 4.63 ppm for T15 and A30, respectively, Table II) maintained their characteristic upfield shifts, relative to the analogous protons in the other nucleotides.

All nine adenosine H2 protons of the ABP-modified duplex were detected in D_2O at 5 °C by 1D inversion–recovery experiments and assigned in a similar manner as described for the unmodified duplex. The signal at 7.62 ppm was identified as the adenosine H2 proton of the terminal A30, since it displayed a weak NOE to its own sugar H1′ proton (peak g, Figure 4b-I) in the NOESY spectrum recorded in D_2O buffer. The remaining resonance a 7.69 ppm was then assigned to the H2 proton of A16. As mentioned before, the chemical shift discrepancies noted for the adenosine H2 protons between Tables I and II could be attributed to a combination of solvent and temperature effects.

The most notable feature in the D_2O spectrum of the modified duplex was that the cross peaks corresponding to the NOEs between the base protons or the sugar H1′ protons and the sugar H2′, H2″, and H3′ protons of the bases at ([ABP]-G11:C20) or near (T9–T10) the modification site were either absent or too weak to be detected. Similarly, definite assignments were not possible for the sugar H2′, H2″, and H3′ protons belonging to the central C5–T6–T7–C8 segment in the ABP-modified strand since the cross peaks were extensively overlapped. The remaining nonexchangeable sugar H2′, H2″, and H3′ protons could be assigned by combined analyses of the COSY and NOESY spectra.

The chemical shift variations that were detected as a result of the ABP-adduct formation were minor for nucleotides located away from the modification site. When compared to the analogous nucleotides in the corresponding unmodified duplex (Table II), the base and sugar protons of the ABP-modified duplex were generally shielded less than 0.1 ppm, which may be due to a temperature effect. However, the base H8 and the sugar H2′ protons of A21, adjacent to the modification site in the opposite strand, were shielded to a greater extent (+0.23 and +0.30 ppm, respectively). In contrast, the sugar H1′ protons of T9, T10, and [ABP]G11, as well as that of C20, located across the ABP-modified G11 in the [ABP]G11:C20 base pair, were deshielded, with the latter having the largest effect (–0.32 ppm). Taken together, these observations suggest that a certain extent of structural perturbation exists in the vicinity of the modification site.

Assignment of the ABP Protons

Major Conformer. The nine aromatic protons in the ABP moiety of [ABP]G11 can be classified into two separate spin systems on the basis of their scalar-coupling networks and molecular symmetry. Thus, the H3,5 and H2,6 protons of the aromatic ring directly attached to G11 were expected to form a strongly coupled AA′BB′ system, while the H2′,6′, H3′,5′, and H4′ protons in the other ring would make an isolated AA′BB′C system (Chart II). Figure 6b shows an expanded portion of the symmetrical aromatic region from a 300-ms NOESY spectrum recorded in D_2O buffer, which established the scalar-coupled interactions between the ABP aromatic protons (peaks A–D) as well as several interbase NOE connectivities (peaks a–i). The former interactions were readily recognized because of their identical appearance in the COSY spectrum (not shown), which exhibited only cross peaks stemming from the fixed scalar-coupled ABP aromatic protons. A similar pattern of contour plots was obtained in an 80-ms NOESY spectrum (Figure 6c), in which most of the interbase cross peaks were too weak to be detected.

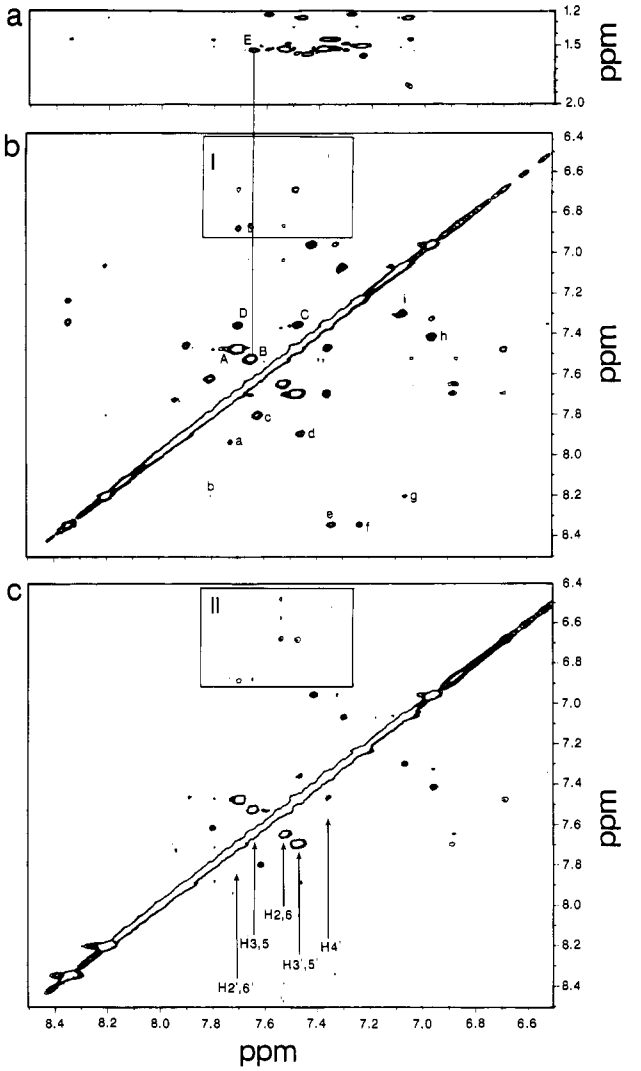

FIGURE 6: Expanded phase-sensitive NOESY contour plots of the ABP-modified 15-mer duplex in D_2O buffer at 5 °C. Spectrum a, establishing the NOE connectivities between the aromatic protons (6.5–8.5 ppm) and thymidine methyl protons (1.2–2.0 ppm), was obtained using a 300-ms mixing time. Spectra b and c were recorded using mixing times of 300 and 80 ms, respectively, and establish NOE connectivities in the aromatic region (6.5–8.5 vs 6.4–8.5 ppm). Cross peaks in the boxed regions I and II are discussed in the text. The assignments of the labeled cross peaks are as follows: A, ABP-(H2′,6′–H3′,5′); B, ABP(H3,5–H2,6); C, ABP(H3′,5′–H4′); D, ABP-(H2′,6′–H4′); E, ABP(H3,5)–T10(Me); a, G17(H8)–A16(H8); b, A2(H2)–A30(H8); c, A30(H2)–A2(H2); d, G28(H8)–A27(H8); e, C3(H6)–A2(H8); f, T1(H6)–A2(H8); g, T29(H6)–A30(H8); h, A21(H2)–A22(H2); i, A24(H2)–A25(H2).

Table III: Comparison of the Aromatic Proton Chemical Shifts of ABP, dG-C8-ABP, and ABP in 15-mer Single Strand and Duplex

compound	H2′,6′	H2,6	H3,5	H3′,5′	H4′
ABP[a]	7.53	7.60	6.75	7.39	7.26
dG-C8-ABP[b]	7.61	7.57	7.79	7.42	7.28
ABP in 15-mer single strand[c]	7.50	7.34[d]	7.51[d]	7.35	7.24
ABP in 15-mer duplex, major[c]	7.71	7.52	7.65	7.48	7.36
ABP in 15-mer duplex, minor[c]	6.88	6.70[d]	6.88[d]	6.70	6.52

[a] Measured in $CDCl_3$. Chemical shifts are reported downfield from TMS. [b] Measured in dimethyl sulfoxide-d_6. Chemical shifts are reported downfield from TMS. [c] Measured in D_2O buffer. Chemical shifts are reported downfield from TSP. Major and minor refer to the two conformations that are in slow exchange (see text). [d] Assignments may be interchanged.

The 7.65 and 7.52 ppm resonances, which formed a strong AA′BB′ system, were assigned to the H3,5 and/or H2,6 protons (peak B, Figure 6b), while the resonances at 7.71, 7.48, and 7.36 ppm, which formed an isolated AA′BB′C system, were readily assigned to the H2′,6′, H3′,5′, and H4′ protons, respectively (peaks A, C, and D, Figure 6b). The latter assignment was also based on the assumption that the most upfield resonance corresponded to the *para*-H4′ proton (Chart II). An essentially identical NOE pattern for the protons of the ABP moiety was also detected in the aromatic region of the NOESY spectrum recorded in H_2O buffer (box I, Figure 5). However, the NOE cross peaks arising from the interactions of the H4′ proton to the H3′,5′ protons (peak C, Figure 6b) and to the H2′,6′ protons (peak D, Figure 6b) were not detectable in Figure 5, presumably due to a low resolution.

We attempted an unambiguous assignment of the H2,6 and H3,5 protons of the strongly coupled AA′BB′ system based on the NOESY experiments. These protons should be in close proximity to the nucleic acid protons at the modification site and thereby provide crucial information on the orientation of the ABP ring. However, their definite assignment was hampered primarily by the lack of suitable long-range interactions between the protons in the two rings of the ABP moiety. In a model study with the parent unadducted amine, ABP, using deuterated chloroform as the solvent (Table III), we were able to detect a weak NOE between the H2,6 and H2′,6′ protons that are spatially close to each other (not shown). On the basis of this model experiment, we obtained an additional NOESY spectrum with a longer mixing time (500 ms), in an attempt to detect the same type of NOE, but the data and their interpretation were not conclusive, owing to poor resolution. Similarly, a parallel model study with the ABP-modified single strand (not shown) did not establish a definite assignment of the H2,6 and H3,5 protons (Table III). We found, however, that for the ABP-modified duplex the downfield ABP proton signal of the AA′BB′ system at 7.65 ppm revealed an NOE to the T10 methyl protons (peak E, Figure 6a). This is significant, since such a cross peak could conceivably only arise from the interaction between the methyl protons of T10 and the ABP H3,5 but not the H2,6 protons. An additional experiment was conducted with dG-C8-ABP, using deuterated dimethyl sulfoxide as the solvent. On the basis of an NOE resulting from saturation of the ABP NH proton, the H2,6 protons were determined to be upfield of the H3,5 protons (Table III). These data confirm the results of an earlier study (Kadlubar et al., 1982). A similar experiment could not be conducted with the ABP-modified duplex because the exchangeable NH proton that bridges the ABP ring and the C8 position of G11 was not detected, perhaps due to rapid exchange with H_2O. After considering all these data, we assigned the 7.52 and 7.65 ppm resonances to the H2,6 and H3,5 protons, respectively, in the ABP-modified duplex.

Despite some ambiguity encountered in the H2,6 and H3,5 proton assignments for the ABP-modified single strand (vide supra), it could be safely concluded that all the ABP ring protons were consistently deshielded upon duplex formation (Table III). This indicated that the adduct in the modified duplex did not significantly stack with the neighboring bases. Our observation contrasts with previous data on ABP-modified dimeric and tetrameric single strands, in which some extent of stacking interactions was found between the ABP moiety and the adjacent bases (Shapiro et al., 1986; Lasko et al., 1987).

Minor Conformers. A second set of NOE cross peaks associated with the ABP resonances was detected in the 7.3–7.9 vs 6.5–7.1 ppm region of the NOESY spectra of the ABP-modified duplex, recorded both in H_2O (box II, Figure 5) and D_2O buffer (box I, Figure 6b). Curiously, the observed intensities of these NOEs were stronger in the spectrum recorded in H_2O buffer. These cross peaks displayed NOE interactions to the ABP protons of the major conformer and not to any nucleic acid protons. Thus, the NOEs must have resulted from saturation transfer between the ABP protons of the major and one or more minor conformers, which were presumably in slow exchange. This was confirmed by recording a short mixing time (80-ms) NOESY spectrum in D_2O buffer, in which spin diffusion effects were reduced significantly. As a result, we could relate each cross peak in box II (Figure 6c) to the corresponding ABP ring protons of the major conformer. Hence, we assigned the 6.52, 6.70, and 6.88 ppm resonances, respectively, to the H4′, H3′,5′, and H2′,6′ protons of the AA′BB′C system in a minor conformer. By the same token, the 6.70 and 6.88 ppm resonances were assigned, respectively, to the H2,6 and H3,5 protons of the isolated AA′BB′ system in the ABP ring of the minor conformer. The chemical shifts of H3,5 and H2′,6′ (6.88 ppm), as well as those of H2,6 and H3′,5′ (6.70 ppm), were degenerate (Table III).

The above observations clearly indicated that at least one minor conformation exists in slow exchange with the major conformer (vide infra). It is noteworthy that the ABP protons of the minor conformer(s) were uniformly shielded by about 1 ppm relative to the corresponding protons of the major conformer. Thus, it appears that the orientation of the ABP moiety in the minor conformer(s) is substantially different from that prevalent in the major conformer, which results in more disruption of the helix. We estimate the amount of the minor conformer to be 5–10% of the total.

Temperature Dependence of the Nonexchangeable Cytidine Base Protons. In the course of recording the COSY and NOESY spectra of the ABP-modified duplex at various temperatures, we noted that the nonexchangeable protons of certain cytidines were quite temperature sensitive. No such dependence was detected for other nonexchangeable protons. The temperature dependence of the cytidine resonances is clearly illustrated in Figure 7, which shows an expanded region (7.0–8.5 vs 5.0–6.5 ppm) of the COSY spectra of the ABP-modified 15-mer duplex, recorded in D_2O buffer at three different temperatures (5, 20, and 27 °C). The only expected cross peaks in this region are the scalar-coupling interactions between the cytidine H5 and H6 protons. In accord with the expectation, all the cross peaks corresponding to the six cytidines were detected at 5 °C, with two of them (C5 and C8) overlapping (Figure 7a). The unambiguous assignment of these resonances has already been discussed (see Figures

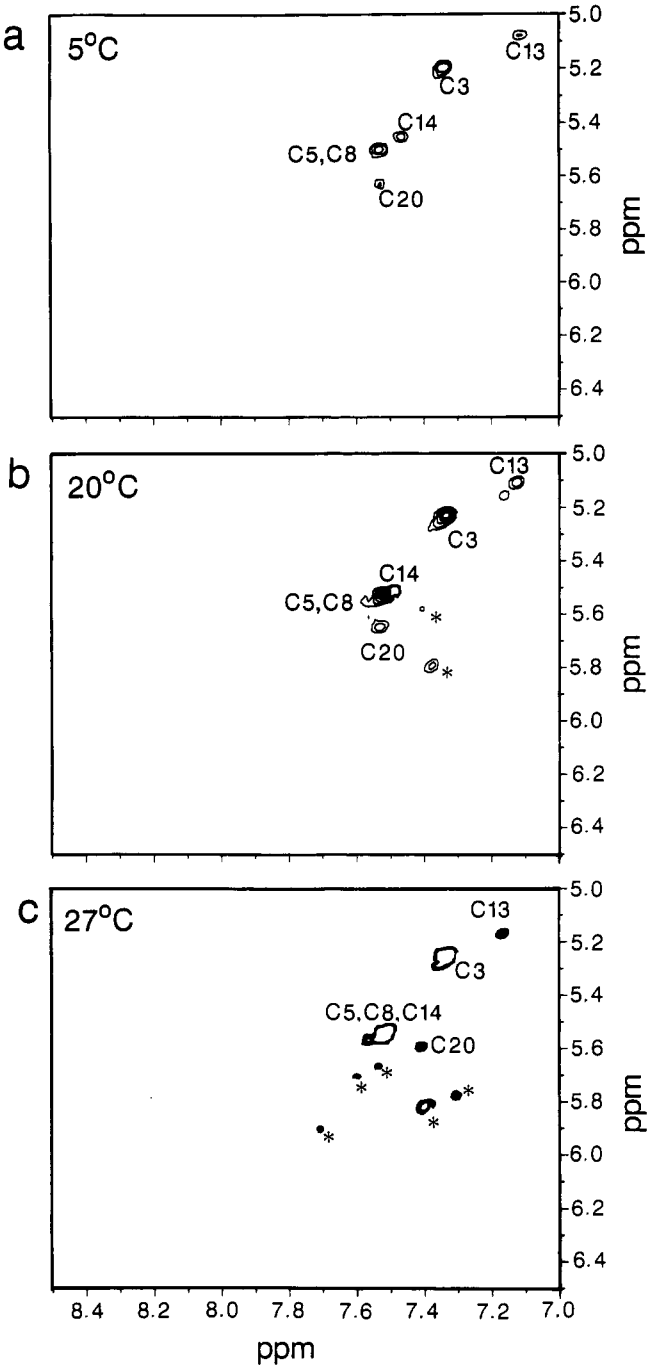

FIGURE 7: Expanded COSY contour plots of the ABP-modified 15-mer duplex in D_2O buffer at (a) 5, (b) 20, and (c) 27 °C. Cross peaks establish the scalar connectivities between cytidine H5 and H6 protons. Analogous interactions due to minor conformations are designated by asterisks.

4b and 5). At the higher temperature (27 °C, Figure 7c), the chemical shifts of these nonexchangeable cytidine H5 and H6 protons were changed, with those at (C20) or near (C13 and C14) the modification site having a greater effect. It should be mentioned, however, that the temperature-dependent chemical shift changes observed for the C13 and C14 residues were probably in part due to the terminal fraying effects. It is also interesting to note that while the H5 and H6 protons of C13 and C14 in the ABP-modified strand were deshielded upon raising the temperature, those of C20, which opposes [ABP]G11, were shielded. These chemical shift transitions were progressive, as was clearly reflected by inspecting the COSY spectrum recorded at the intermediate temperature (20 °C, Figure 7b).

In addition to these observations, we were able to detect several extra cross peaks not belonging to the cytidine H5–H6 protons of the main conformer. Some of these cross peaks are marked by asterisks in Figure 7b,c. Since we did not expect any other scalar couplings in this region, the extra cross peaks must have originated from identical interactions involving cytidine protons of the minor conformer(s). This further substantiated the earlier conclusions about the existence of minor conformers, drawn from analyses of the ABP ring resonances and the imino proton resonances (vide supra).

It is also significant that, regardless of the temperature, the COSY cross peaks between the H5 and H6 protons of both C13 and C20 were noticeably weaker than those of the other cytidines, including their counterparts in the unmodified duplex. This could be due to decreased mobility of the cytidine residues in the vicinity of the modification site as a consequence of conformation averaging between different duplex conformers. For example, Borah et al. (1985) have reported that the intensities of the cross peaks between the cytidine H5 and H6 protons in nucleotides are highly sensitive to the local environment and mobility of the oligomers, presumably due to spin diffusion effects.

DISCUSSION

The present NMR study has focused on the conformational perturbation induced by a single dG-C8-ABP adduct in a 15-mer sequence spanning a portion of the mouse c-Ha-*ras* protooncogene centered around codon 61. The structural consequences of ABP adduct incorporation were examined by conducting a comparative analysis of the NMR characteristics of the ABP-modified 15-mer and the parent duplex. This study represents the first structural elucidation of a DNA duplex containing one [ABP]G:C base pair. At least two conformations were found to exist in a slow to intermediate rate of exchange on the NMR time scale. Only the major conformation was characterized in detail, but some structural features of the minor conformer(s) could also be inferred from our data.

Structure of the Unmodified 15-mer Duplex

Several lines of evidence established that the unmodified duplex adopts a standard right-handed B-type DNA conformation in solution, with every base pair in the normal Watson–Crick configuration, with the possible exception of the fraying terminal ends.

Stepwise end-to-center thermal broadening of the eleven partially resolved imino protons observed in the H_2O spectrum (Figure 3a) indicated the formation of a standard double-helical duplex in agreement with our previous optical results (Marques & Beland, 1990). Evidence for Watson–Crick pairing of the nonterminal bases stems from the presence of characteristic imino proton resonances in the 12.0–14.5 ppm region, as well as from the observed NOE connectivities between each imino proton and the corresponding protons across the base pair (Figure 2a-II). Thus, NOE cross peaks were detected between each of the six well-resolved thymidine imino protons and the H2 proton of its opposite adenosine, which is consistent with the formation of Watson–Crick A27:T4, A25:T6, A24:T7, A22:T9, A21:T10, and A12:T19 base pairs. Similarly, all the five internal guanosine imino protons, which were well resolved at 5 °C, exhibited NOEs to the amino and H5 protons of their opposite cytidines, which indicated the formation of Watson–Crick G28:C3, G26:C5, G23:C8, G11:C20, and G18:C13 base pairs. Furthermore, the chemical shift separations (1.2–1.8 ppm) between the

hydrogen-bonded and exposed cytidine amino protons were within the typical range found in Watson–Crick base pair configurations (Boelens et al., 1985).

The directionality of the duplex could, in turn, be inferred from the cross peaks observed in the NOESY spectra of the unmodified 15-mer recorded in D_2O buffer (Figure 4a). The sequential intrastrand connectivities between the purine H8 or pyrimidine H6 protons and their own and the 5′-adjacent sugar H1′ protons unambiguously established the formation of a regular right-handed helix. The observation that some adenosine H2 protons displayed weak NOEs to sugar H1′ protons of the partner strand was also a characteristic marker for a right-handed helix (Weiss et al., 1984). In addition, the fact that the NOEs detected between each base H8/H6 proton and its own sugar H1′ proton were much weaker than those reflecting cytidine H5–H6 interactions indicated that every residue in the unmodified duplex adopts an anti configuration about the glycosyl bond.

Our NMR data thus provided sufficient evidence that, with the possible exception of the fraying terminal base pairs, the unmodified duplex assumes a right-handed B-type DNA conformation in solution.

Structure of the ABP-Modified 15-mer

Global Structure of the ABP-Modified 15-mer Duplex. The structural effects of ABP-adduct formation at the C8 position of a single guanosine in the modified duplex were first examined by comparison of the spectral pattern of the exchangeable protons with the corresponding region in the unmodified duplex. As shown in Table I, the chemical shift changes that occurred for the adenosine H2 and the exchangeable protons as a consequence of adduct formation at 5 °C were almost negligible (≤0.07 ppm), with the exception of those in the base pairs at or near the modification site. This indicated that the structural alterations caused by the adduct formation were small and localized. With the exception of the amino protons of C20 in the [ABP]G11:C20 base pair (Table I), we detected virtually no chemical shift variations of the cytidine amino protons. In addition, the fact that the chemical shift separation of the hydrogen-bonded and exposed amino protons of cytidine was in the range of 1.2–1.8 ppm suggested that the Watson–Crick base pair configuration found for the unmodified duplex was still intact in the ABP-modified duplex.

In full consistency with these arguments, the general pattern of NOE connectivities observed for both duplexes in the 200-ms NOESY spectra recorded in H_2O buffer at 5 °C was strikingly similar (Figure 2a,b). This indicated that both species assume analogous B-type DNA conformations in solution. Also, as found for the unmodified duplex, the imino protons of the terminal A:T base pairs were strongly attenuated due to fraying, even at 5 °C. The seven internal thymidine imino protons of the A:T base pairs, including those near or flanking the modification site (e.g., A22:T9, A21:T10, and A12:T19), exhibited characteristic NOEs to the H2 protons of their partner adenosines. Similarly, the internal guanosine imino protons exhibited characteristic NOEs to the amino and H5 protons of their partner cytidines, as well as to the adenosine H2 protons of flanking A:T base pairs. The lack of the cross peaks corresponding to [ABP]G11(NH)–A21(H2) and to G17(NH)–C14(H5) (Figure 2b-II) was the only exception to this general pattern. These data clearly indicated that every single base pair in the modified oligomer, with the possible exception of modification site, adopts the normal Watson–Crick base pair configuration.

The NOE connectivities between the base H8/H6 and the sugar H1′ protons, observed in the NOESY spectra of the ABP-modified duplex in D_2O buffer at 5 °C (Figure 4b), displayed a directionality from which we could deduce the handedness of the modified helix. Again, with the exception of the segments near the modification site, the NOE patterns were quite similar in both duplexes. We could trace the NOE cross peaks along the entire oligonucleotide chains, with an interruption at the C8 position of G11, where there was no base proton due to the covalent ABP modification. The observed NOEs between the base protons and their own and 5′-linked sugar protons, along with the interbase NOEs between adjacent base protons (A2–C3, A12–C13, C13–C14, and T19–C20) and between the adenosine H2 protons and the sugar H1′ protons on the coding strand (Figure 4b) established the presence of a right-handed helix, with all bases stacked into the duplex (Weiss et al., 1984). In addition, the minor groove adenosine H2 protons were virtually unaffected upon ABP modification, with the exception of those belonging to A12 and A22 (downfield shifts of –0.12 and –0.17 ppm, respectively, Table I), which are located adjacent and two base pairs away from the modification site, respectively. These results further supported that the structural perturbation arising from ABP modification of the parent duplex was weak and localized, with the ABP-modified duplex retaining the overall characteristics of a standard B-type DNA configuration.

[ABP]G11(anti):C20(anti) Watson–Crick Base Pairing. The proton assignments of the ABP-modified 15-mer duplex have not been completed, particularly with regard to most of the sugar protons at and near the modification site (see Table II). However, we have sufficient information to propose the conformational alignment of the [ABP]G11:C20 base pair and the orientation of the ABP ring in neutral aqueous solution. While it can be concluded that the presence of the [ABP]-G11:C20 base pair in the ABP-modified duplex caused no significant overall structural perturbation (vide supra), we did observe subtle local conformational distortions around [ABP]G11, as compared to the vicinity of G11 in the parent duplex. For example, the temperature dependence of the imino protons indicated that although the melting of the parent duplex started from the ends, the ABP-modified duplex opened at both the ends and the adduct site. This abnormal duplex opening near the site of modification was further supported by the results from the temperature dependence of COSY and NOESY spectra that were recorded at 5, 20, and 27 °C (vide supra).

The NOE connectivities and the chemical shift changes found for the imino, base, and sugar protons in the (T10–[ABP]G11–A12)·(A21–C20–T19) segment provided crucial information about the structural constraints at the modification site. While the imino proton of G11 in the [ABP]G11:C20 base pair of the ABP-modified duplex exhibited a moderate upfield shift (+0.09 ppm), possibly reflecting a slight decrease in the extent of hydrogen bonding, a rather substantial upfield shift (+0.54 ppm) was observed for the imino proton of T10 in the A21:T10 base pair, located next to the adduct site. Moderate downfield shifts (–0.09 ppm), possibly reflecting small changes in the stacking interactions, were in turn detected for the imino protons of the A22:T9 and A12:T19 base pairs, located within close proximity of the adduct site. Despite these perturbations, the imino proton of the ABP-modified G11 displayed NOE interactions that were characteristic of a standard Watson–Crick base pair configuration. Specifically, it developed strong NOEs to the hydrogen-bonded (peak 13, Figure 2b-II) and exposed (peak 19, Figure 2b-II) amino protons of C20 (8.79 and 6.99 ppm, respectively). It also displayed an NOE to the H2 proton of the 3′-flanking A12

(peak 3, Figure 2b) but not to that of the 5′-flanking A21, in the opposite strand. This latter finding indicated a possible conformational alteration in the A21:T10 base pair.

In addition to establishing [ABP]G11:C20 as an almost intact base pair, the above-discussed results further indicated that the guanosine fragment of [ABP]G11 was incorporated into the helix in a standard manner, assuming a normal anti glycosidic torsion angle, which was also adopted by the flanking bases. It should be stressed that both amino protons of C20 were significantly deshielded (–0.20 and –0.26 ppm, for the exposed and hydrogen-bonded amino protons, respectively), in contrast to the amino protons of the remaining cytidines that, being relatively distant from the modification site, remained virtually unaffected (≤0.06 ppm) upon ABP modification. Interestingly, however, the chemical shift separation (1.80 ppm) observed between the C20 amino protons in the [ABP]G11:C20 base pair was in a comparable range (1.74 ppm) to that observed in the unmodified G11:C20. Thus, while this separation is thoroughly consistent with participation of C20 in hydrogen bonding with the modified G11, the observed downfield shifts may reflect a decrease in the extent of stacking interactions involving C20. They may also imply that the Watson–Crick [ABP]G11(anti):C20(anti) base pair slips slightly out of the main helical axis, which results in local distortion at the modification site. This could explain the substantial upfield shifts observed for the H8 proton of A21 and the imino and methyl protons of T10 in the A21:T10 base pair (see Tables I and II), although ABP phenyl ring-current effects could contribute partly to the effect found with the T10 methyl protons.

Interestingly, the effect upon the ABP modification was far more significant for the A21:T10 base pair, flanking the modification site in the 5′ direction, than for the A12:T19 base pair, which flanks the same position in the 3′ direction (vide supra). This may be related to a sequence-dependent phenomenon rather than to the nature of the ABP ring, due to the fact that while A21:T10 is stacked with another A:T base pair (A22:T9) in the 5′ direction, A12:T19 is adjacent to a G:C base pair (G18:C13) in the 3′ direction. Since the hydrogen-bonding potential of a G:C base pair is much greater than that of an A:T pair, it is conceivable that the segment containing a higher G:C content is more resistant to the conformational damages caused by adduct incorporation. Nonetheless, the NOEs between the H5 proton of C20 and the H6 (peak h, Figure 4b) and methyl protons of the 5′-neighboring T19 (not shown), found in the NOESY spectra of the modified duplex in D_2O buffer, allowed us to conclude that C20 remains stacked into a right-handed T19–C20–A21 segment. The weak NOE between the H6 proton of C20 and its own sugar H1′ proton, when compared with the strong cross peaks between the H5 and H6 protons of individual cytidines in the 80-ms NOESY spectrum (not shown), is also consistent with C20 assuming an anti conformation about the glycosyl bond in the modified duplex (vide supra). Thus, taken together, these NMR data indicated that both components of the base pair at the modification site adopt a standard anti conformation about the glycosyl bond.

Orientation of the ABP Moiety

Major Conformer. With the exception of the exchangeable NH proton that bridges the ABP ring moiety and the C8 position of G11 in the modified duplex (Chart II), we located all the protons belonging to the ABP system. The five resonances observed for the ABP ring corresponded to degenerate spin systems (i.e., AA′BB′ and AA′BB′C), which indicated that the ring moiety was rapidly rotating. In addition, we detected an NOE cross peak between the H3,5 protons of ABP and the methyl protons of T10 (peak E, Figure 6a), which serves as additional important evidence for an [ABP]G11(anti):C20(anti) configuration at the modification site. No other obvious NOE connectivities involving the ABP ring system and nucleic acid protons were detected. Furthermore, all of the ABP ring protons experienced downfield shifts upon duplex formation (Table III), which strongly indicated that the ABP in the major conformation was not stacked with neighboring bases. Since the arylamine fragment in the major conformer did not appear to be involved in any stacking interactions with the helix, these results were consistent with a preferred positioning of the ABP ring in the major groove of a weakly perturbed duplex.

Minor Conformer(s). The observation of exchange cross peaks involving the ABP ring protons, as well as the direct observation of several subspectra and extra COSY peaks stemming from cytidine H5–H6 interactions, are evidence for the presence in solution of at least one minor conformer of the ABP-modified duplex. The apparent slow equilibrium between the major conformer discussed above and these minor contributors was clearly temperature dependent, with the major conformer being more pronounced in the lower temperature range. We were not able to obtain sufficient data on the minor conformer(s) to enable us to make a thorough structure elucidation; however, it should be emphasized that the ABP ring protons of the minor conformer(s) consistently exhibited upfield shifts (about 1 ppm) from their analogous protons in the major conformer. This could be interpreted as indicating that the ABP ring in the minor conformer(s) is under the influence of extensive stacking interactions. One possibility consistent with this extensive stacking is the adoption of a syn conformation by the ABP-modified G11, with the consequent insertion of the arylamine fragment into the helix. However, as with the major conformer, it appears that the ABP ring is rapidly rotating. Alternatively, a Hoogsteen type base pairing could be adopted, with the ABP moiety residing in the minor groove, as was observed for an AF-modified syn guanosine opposing an anti adenosine in a 12-mer duplex (Norman et al., 1989; Broyde et al., 1990).

Previous studies have shown that the sugar ring of the related DNA adduct dG-C8-AF has a high C2′-endo population and possibly an unusual O4′-endo conformation (Evans et al., 1980; Evans & Levine, 1987). Since dG-C8-AF and dG-C8-ABP have similar sugar conformations (Kadlubar et al., 1982), if these conformations are present in the ABP-modified duplex, they could be responsible, in part, for the flexibility at the modification site and the minor conformer(s) that are observed. The partial characterization of the minor conformer(s) of the ABP-modified duplex is of particular interest since the structural perturbation is clearly more dramatic and because stacking of this class of carcinogen adducts provides a possible mechanism for mutations (Shapiro et al., 1986; Evans & Levine, 1988).

Summary

From the present NMR studies, we conclude that the ABP modification of a complementary 15-mer duplex caused an equilibrium between at least two different conformations that is relatively slow on the NMR time scale. For the major conformer, the structural alterations were weak, temperature dependent, and localized to the immediate vicinity of the modification site, where the base and sugar protons showed somewhat significant chemical shift changes. The effect was greater in the 5′ direction of the modified strand, in what may be a sequence-dependent phenomenon. The standard Watson–Crick type base pairing was not seriously disturbed throughout the entire length of the ABP-modified duplex, and all the

glycosidic torsion angles had normal anti conformations. As a result, the arylamine was predicted to reside in the major groove of a relatively undistorted helix and undergo rapid rotation. We did not observe any evidence of carcinogen–base stacking interactions in the major conformer. Our experimental results on the major conformer thus strongly support previous predictions (Shapiro et al., 1986) that the dG-C8-ABP adduct should reside in the major groove, without serious perturbation of the double-helical structure. This absence of a strong conformational disturbance might prevent the recognition of the ABP lesion by mammalian repair enzymes, thereby facilitating the onset of the carcinogenic response. However, minor conformer(s), for which the ABP moiety may be stacked with neighboring bases or situated in the minor groove, were observed, and these became more important at temperatures closer to the physiological temperature range. The possibility of a biological significance of these minor contributors(s), therefore, cannot be ruled out. In this regard, we wish to make note of our preliminary findings from two duplexes containing dG-C8-AF in place of dG-C8-ABP. In one case, the same 15-mer was under investigation, and we found that both the ABP- and AF-modified duplexes adopt a similar major conformation but that the contribution of the minor conformer(s) was much greater in the AF-modified duplex. In another AF-modified duplex, with a different length (9-mer) and a different sequence, with a higher G:C content, we also found more than one conformation, with the population of the minor conformer(s) being higher still than in either 15-mer. These preliminary results indicate that sequence, the nature of the carcinogen, and possibly the length of the DNA duplex will affect the distribution of conformers in duplexes with this type of modification.

ACKNOWLEDGMENT

We thank Robert A. Levine for his technical assistance.

REFERENCES

Abuaf, P. A., Kadlubar, F. F., & Grunberger, D. (1987) *Nucleic Acids Res. 15*, 7125–7136.

Anderson, M. W., & Reynolds, S. H. (1989) in *The Pathobiology of Neoplasia* (Sirica, A. E., Ed.) pp 291–304, Plenum Press, New York.

Aue, W. P., Bartholdi, E., & Ernst, R. R. (1976) *J. Chem. Phys. 64*, 2229–2246.

Beland, F. A., & Kadlubar, F. F. (1990) in *Handbook of Experimental Pharmacology* (Cooper, C. S., & Grover, P. L., Eds.) Vol 94/I, pp 267–325, Springer-Verlag, Heidelberg.

Beland, F. A., Fullerton, N. F., Smith, B. A., & Poirier, M. C. (1992) in *Relevance of Animal Studies to the Evaluation of Human Cancer Risk* (D'Amato, R., Slaga, T. J., Farland, W. H., & Henry, C., Eds.) pp 79–92, Wiley-Liss, New York.

Bodenhausen, G., Kogler, H., & Ernst, R. R. (1984) *J. Magn. Reson. 58*, 370–388.

Boelens, R., Scheek, R. M., Dijkstra, K., & Kaptein, R. (1985) *J. Magn. Reson. 62*, 378–386.

Borah, B., Roy, S., Zon, G., & Cohen, J. S. (1985) *Biochem. Biophys. Res. Commun. 133*, 380–388.

Broyde, S., & Hingerty, B. (1983) *Biopolymers 22*, 2423–2441.

Broyde, S., & Hingerty, B. E. (1987) *Nucleic Acids Res. 15*, 6539–6552.

Broyde, S., Hingerty, B. E., & Srinivasan, A. R. (1985) *Carcinogenesis* 6, 719–725.

Broyde, S., Hingerty, B. E., Shapiro, R., & Norman, D. (1990) in *Nitroarenes: Occurrence, Metabolism, and Biological Impact* (Howard, P. C., Hecht, S. S., & Beland, F. A., Eds.) pp 113–123, Plenum Press, New York.

Evans, F. E., & Miller, D. W. (1982) *Biochem. Biophys. Res. Commun. 108*, 933–939.

Evans, F. E., & Levine, R. A. (1986) *J. Biomol. Struct. Dyn. 3*, 923–934.

Evans, F. E., & Levine, R. A. (1987) *Biopolymers 26*, 1035–1046.

Evans, F. E., & Levine, R. A. (1988) *Biochemistry 27*, 3046–3055.

Evans, F. E., Miller, D. W., & Beland, F. A. (1980) *Carcinogenesis 1*, 955–959.

Evans, F. E., Miller, D. W., & Levine, R. A. (1984) *J. Am. Chem. Soc. 106*, 396–401.

Famulok, M., Bosold, F., & Boche, G. (1989) *Angew. Chem., Int. Ed. Engl. 28*, 337–338.

Fazakerley, G. V., van der Marel, G. A., van Boom, J. H., & Guschlbauer, W. (1984) *Nucleic Acids Res. 12*, 8269–8279.

Feigon, J., Leupin, W., Denny, W. A., & Kearns, D. R. (1983) *Biochemistry 22*, 5943–5951.

Hare, D. R., Wemmer, D. E., Chou, S.-H., Drobny, G., & Reid, B. R. (1983) *J. Mol. Biol. 171*, 319–336.

Hingerty, B. E., & Broyde, S. (1982) *Biochemistry 21*, 3243–3252.

Hingerty, B., & Broyde, S. (1986) *J. Biomol. Struct. Dyn. 4*, 365–372.

Hore, P. J. (1983) *J. Magn. Reson. 55*, 283–300.

Kadlubar, F. F., Beland, F. A., Beranek, D. T., Dooley, K. L., Heflich, R. H., & Evans, F. E. (1982) in *Environmental Mutagens and Carcinogens* (Sugimura, T., Kondo, S., & Takebe, H., Eds.) pp 385–396, Liss, New York.

Krugh, T. R., Sanford, D. G., Walker, G. T., & Huang, G. (1987) *Pontif. Acad. Sci. Scr. Varia 70*, 147–168.

Lasko, D. D., Basu, A. K., Kadlubar, F. F., Evans, F. E., Lay, J. O., Jr., & Essigmann, J. M. (1987) *Biochemistry 26*, 3072–3081.

Leng, M., Ptak, M., & Rio, P. (1980) *Biochem. Biophys. Res. Commun. 96*, 1095–1102.

Lipkowitz, K. B., Chevalier, T., Widdifield, M., & Beland, F. A. (1982) *Chem.-Biol. Interact. 40*, 57–76.

Marques, M. M., & Beland, F. A. (1990) *Chem. Res. Toxicol. 3*, 559–565.

Neidle, S., Kuroda, R., Broyde, S., Hingerty, B. E., Levine, R. A., Miller, D. W., & Evans, F. E. (1984) *Nucleic Acids Res. 12*, 8219–8233.

Norman, D., Abuaf, P., Hingerty, B. E., Live, D., Grunberger, D., Broyde, S., & Patel, D. J. (1989) *Biochemistry 28*, 7462–7476.

Patel, D. J., Kozlowski, S. A., Nordheim, A., & Rich, A. (1982) *Proc. Natl. Acad. Sci. U.S.A. 79*, 1413–1417.

Patrianakos, C., & Hoffmann, D. (1979) *J. Anal. Toxicol. 3*, 150–154.

Poirier, M. C., Fullerton, N. F., Kinouchi, T., Smith, B. A., & Beland, F. A. (1991) *Carcinogenesis 12*, 895–900.

Sage, E., & Leng, M. (1980) *Proc. Natl. Acad. Sci. U.S.A. 77*, 4597–4601.

Sanford, D. G., & Krugh, T. R. (1985) *Nucleic Acids Res. 13*, 5907–5917.

Santella, R. M., Grunberger, D., Weinstein, I. B., & Rich, A. (1981) *Proc. Natl. Acad. Sci. U.S.A. 78*, 1451–1455.

Shapiro, R., Underwood, G. R., Zawadzka, H., Broyde, S., & Hingerty, B. E. (1986) *Biochemistry 25*, 2198–2205.

Van Geet, A. L. (1968) *Anal. Chem. 40*, 2227–2229.

van Houte, L. P. A., Bokma, J. T., Lutgerink, J. T., Westra, J. G., Retèl, J., van Grondelle, R., & Blok, J. (1987) *Carcinogenesis 8*, 759–766.

van Houte, L. P. A., Westra, J. G., Retèl, J., & van Grondelle, R. (1988) *Carcinogenesis 9*, 1017–1027.

Vineis, P. (1992) *Cancer Epidemiol. Biomarkers Prev. 1*, 149–153.

Weiss, M. A., Patel, D. J., Sauer, R. T., & Karplus, M. (1984) *Nucleic Acids Res. 12*, 4035–4047.

Wiseman, R. W., Stowers, S. J., Miller, E. C., Anderson, M. W., & Miller, J. A. (1986) *Proc. Natl. Acad. Sci. U.S.A. 83*, 5825–5829.

Wüthrich, K. (1986) *NMR of Proteins and Nucleic Acids*, Wiley-Interscience, New York.